iScience

CellPress
OPEN ACCESS

Article

Landscapes of Protein Posttranslational Modifications of African *Trypanosoma* Parasites

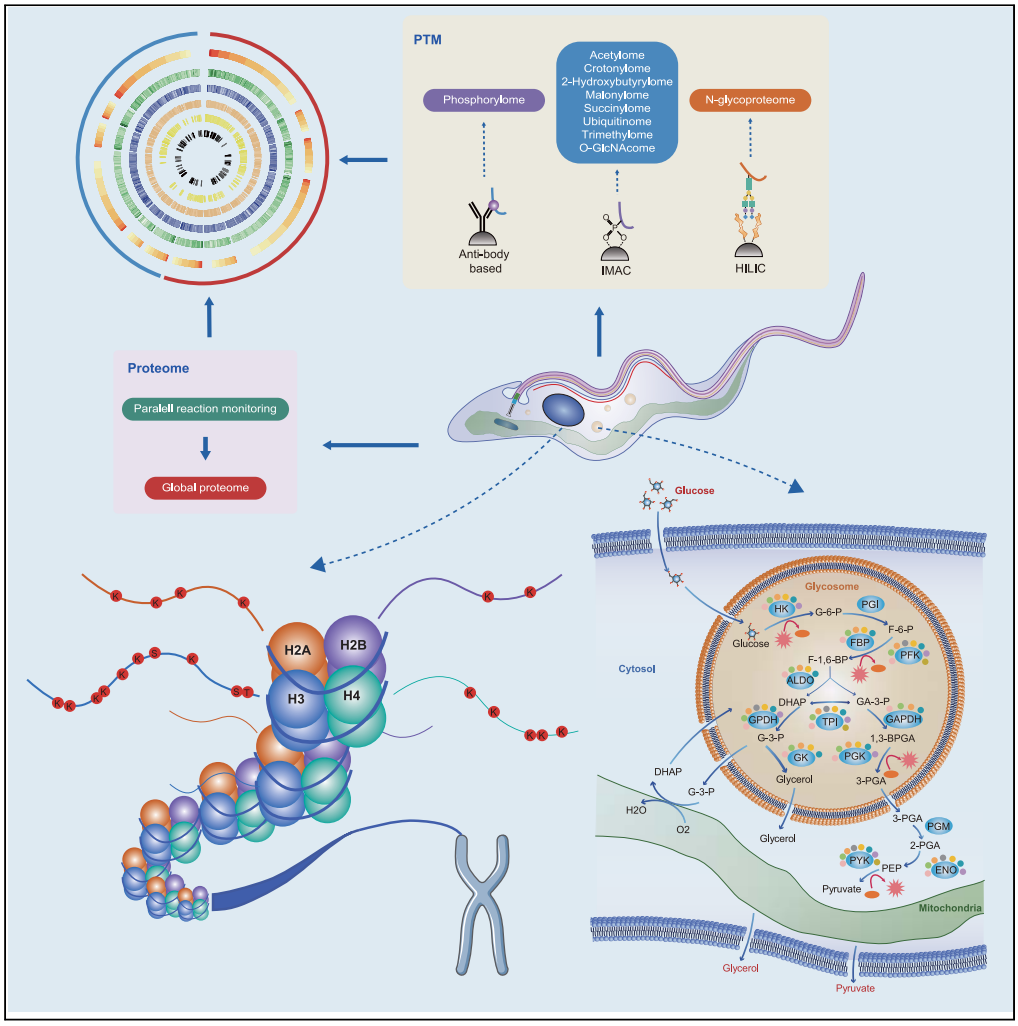

Naiwen Zhang, Ning Jiang, Kai Zhang, ..., Xun Suo, Zhaorong Lun, Qijun Chen

qijunchen759@syau.edu.cn

HIGHLIGHTS

The first multi-proteomic profiles of *T. brucei* and *T. evansi* were generated

Histones are modified heavily and are highly conserved in trypanosomes

The two biologically different trypanosomes displayed distinct PTM-omic features

Crosstalk between different PTMs involved in critical biological processes

DATA AND CODE AVAILABILITY

PXD016245

Zhang et al., iScience *23*, 101074
May 22, 2020
https://doi.org/10.1016/j.isci.2020.101074

iScience

CellPress
OPEN ACCESS

Article

Landscapes of Protein Posttranslational Modifications of African *Trypanosoma* Parasites

Naiwen Zhang,[1,2] Ning Jiang,[1,2] Kai Zhang,[1,2] Lili Zheng,[1,2] Di Zhang,[1] Xiaoyu Sang,[1,2] Ying Feng,[1,2] Ran Chen,[1,2] Na Yang,[1] Xinyi Wang,[3] Zhongyi Cheng,[4] Xun Suo,[5] Zhaorong Lun,[6] and Qijun Chen[1,2,7,*]

SUMMARY

Proteins of all living cells undergo a myriad of post-translational modifications (PTMs) that are critical to multifarious life processes. In this study, we describe the first comprehensive multiple PTM-omics atlas in parallel with quantitative proteome analyses of two representative species of African trypanosomes, *Trypanosoma brucei* and *Trypanosoma evansi*. Ten PTM types with approximately 40,000 modified sites and 150 histone marks with a fine map on each protein of the two African trypanosomes were accomplished. The two biologically different trypanosomal species displayed distinct PTM-omic features, regulation pathways, and networks. Modifications in the proteins involved in the redox system were mainly upregulated in *T. brucei*, whereas proteins associated with motility were predominantly modified in *T. evansi*. The establishment of a database of multiple PTMs in the two parasites provides us with a deep insight into the biological mechanisms that underpin life processes in trypanosomes with different life cycles.

INTRODUCTION

Trypanosomes are vector-borne protozoan parasites that cause substantial mortality and morbidity in mammalian hosts worldwide, and there is no vaccine available for trypanosomiasis (Buscher et al., 2017; Cayla et al., 2019). A subspecies of *Trypanosoma brucei*, *T. b. brucei*, is responsible for the domestic animal disease known as nagana and has been used as a model for various studies due to its close resemblance with the etiologic agents of human sleeping sickness, *T. b. rhodesiense* and *T. b. gambiense*. *Trypanosoma evansi*, the causative agent of the disease surra, is thought to be a mutant of *T. brucei* that has adapted to the gradual loss of kinetoplast DNA and is normally sensitive to human serum (Lai et al., 2008). However, it is now known to be capable of causing infections in humans (Uzureau et al., 2013; Van Vinh Chau et al., 2016; Vanhollebeke et al., 2006), and *T. evansi*-infected monkeys exhibit symptoms similar to those associated with sleeping sickness (Misra et al., 2016), further highlighting its zoonotic potential. Both *T. brucei* and *T. evansi* proliferate predominantly extracellularly within mammalian hosts as bloodstream form (BSF) parasites. Periodic switching of the variant surface glycoprotein coat and concomitant immune evasion results in the generation of waves of parasitemia and long-term survival (Mugnier et al., 2015). However, for polymorphic *T. brucei*, this phenomenon is accompanied by a developmental switch from a slender to a stumpy form; this switch is regulated by quorum sensing (QS) signaling pathways (Mony et al., 2014; Rojas et al., 2019). When the stumpy form parasites are ingested by tsetse flies, the parasites initiate development into the procyclic form (PCF). In contrast, *T. evansi*, which is normally monomorphic, is locked in the slender BSF and incapable of cycling through the insect due to dyskinetoplasty (Carnes et al., 2015; Lai et al., 2008). The mechanical transmission of *T. evansi*, however, enables its infection of a variety of mammalian hosts and transmission beyond Africa, where the obligatory vector of *T. brucei* resides (Jensen et al., 2008).

These two African trypanosomes harbor very similar genomes RNA polymerase II (RNAP II) promoters, and genes are present in polycistronic units (Berriman et al., 2005; Carnes et al., 2015; Zheng et al., 2019). Trypanosomes, therefore, rely almost exclusively on post-transcriptional mechanisms to regulate the output of gene products, highlighting the critical function of RNA-binding proteins (RBPs) (Kolev et al., 2012). Furthermore, the major differences between these two closely related parasites are ultimately caused by dynamic changes in protein homeostasis and post-translational modifications (PTMs). Epigenetic regulation, predominantly through histone modification, is considered as a secondary vehicle for the transmission of heritable messages (Figueiredo et al., 2009). The PTM status of histones and associated variants

[1]Key Laboratory of Livestock Infectious Diseases in Northeast China, Ministry of Education, Key Laboratory of Zoonosis, College of Animal Science and Veterinary Medicine, Shenyang Agricultural University, 120 Dongling Road, Shenyang 110866, China

[2]The Research Unit for Pathogenic Mechanisms of Zoonotic Parasites, Chinese Academy of Medical Sciences, 120 Dongling Road, Shenyang 110866, China

[3]College of Basic Sciences, Shenyang Agricultural University, 120 Dongling Road, Shenyang 110866, China

[4]Jingjie PTM Biolab (Hangzhou) Co. Ltd, Hangzhou 310018, China

[5]National Animal Protozoa Laboratory & College of Veterinary Medicine, China Agricultural University, Beijing 100193, China

[6]State Key Laboratory of Biocontrol, School of Life Sciences, Sun Yat-Sen University, Guangzhou 510275, China

[7]Lead Contact

*Correspondence: qijunchen759@syau.edu.cn

https://doi.org/10.1016/j.isci.2020.101074

Figure 1. Proteomic Profiling and Targeted Verification Reveal Significant Differences of *T. brucei* and *T. evansi*

(A) Flowchart illustrating the proteomic procedures for proteins and modified site identification. Parasite proteins were extracted (step 1) and trypsinized (step 2). One aliquot of peptides was separated by high-performance liquid chromatography (HPLC) (step 3) and analyzed by tandem mass spectrometry (MS/MS) (step 4). A separate aliquot was subjected to affinity enrichment (step 4*) and PTM identification (steps 5* and 6*). The steps marked with asterisks are for PTM analysis. Phosphopeptides were identified by immobilized metal-affinity chromatography (IMAC) (Ficarro et al., 2002), and *N*-glycopeptides

Figure 1. *Continued*

were enriched using a hydrophilic interaction liquid chromatography (HILIC) strategy (Zhang et al., 2016). The other peptides were all enriched using appropriate monoclonal pan-antibodies. Finally, data from all omics sources were combined for bioinformatic analysis (steps 6 and 7*). Parallel reaction monitoring was used to quantify individual unique peptides for targeted validation of the differentially expressed proteins in the two parasites (step 7).

(B) Principal-component analysis (PCA) of the proteome resulted in a clear separation of two groups, representing *T. evansi* and *T. brucei*. The three replicates of the same species clustered tightly.

(C) The quantitative ratio distributions of homologous proteins between *T. brucei* and *T. evansi*.

(D) Venn diagrams illustrating homologous proteins between *T. brucei* (red circle) and *T. evansi* (blue circle). Volcano plot shows the distributions of quantified proteins commonly identified in the two parasites. Highly expressed proteins in *T. brucei* and *T. evansi* are shown in red and blue, respectively, whereas proteins whose expressions were unchanged are shown in pink. Zinc finger proteins (ZFPs) and proteins associated with cell motility, the redox system, and tricarboxylic acid (TCA) cycles are represented by dots of different colors.

(E) Prediction of subcellular localization and classification statistics of the four protein groups.

(F) KEGG pathway-based enrichment of proteins with different expression intensities in *T. brucei* and *T. evansi*. Heatmap colors represent log2-fold changes in expression levels.

See also Figure S1 and Tables S1, S2, and S3.

determines whether chromatin is repressed or activated in relation to transcription and, concomitantly, antigenic variation (Martinez-Calvillo et al., 2018; Muller et al., 2018). Proteomic analyses have already been performed on trypanosomes (Dejung et al., 2016; Roy et al., 2010), and advances in phosphoproteome and acetylome analyses of *T. brucei* have highlighted the role of PTMs in trypanosomes (Moretti et al., 2018; Nett et al., 2009a, 2009b; Urbaniak et al., 2013). However, our knowledge of the molecular biology of *T. evansi* lags way behind that of *T. brucei*. In addition, a global quantitative understanding of associated proteomes and PTM networks is still lacking, and the overall dynamic regulatory mechanisms that facilitate PTMs in trypanosomes remain to be elucidated.

In an effort to better understand the biology of African trypanosomes and unravel the molecular mechanisms that drive developmental differences, we report the first global analysis of multiproteomics for *T. brucei* and *T. evansi* using label-free quantitative techniques. The study also resulted in the generation of a modification-specific proteomic profile that contains the most PTM types in all organisms to date. We further analyzed acylations (acetylation, crotonylation, 2-hydroxyisobutyrylation, malonylation, and succinylation), phosphorylation, trimethylation, ubiquitination, *N*-glycosylation, and *O*-GlcNAcylation on each protein identified, including functional and pathway enrichment and interactive networks. Proteins that are species-specifically expressed and modified were deeply investigated. This study provides a proteome and PTM-ome resource for *Trypanosoma* parasites, which serves as a valuable model to study evolutionarily distinct eukaryotes (Cayla et al., 2019), laying a foundation for the development of new drugs.

RESULTS

Proteomic Profiling and Targeted Verification Reveal Significant Differences of *T. brucei* and *T. evansi*

The proteins of BSF *T. brucei* and *T. evansi* were identified using sophisticated mass spectrometry-based quantitative analysis in three eligible biological replicates; the replicates of the same species cluster tightly in principal-component analysis (PCA) (Figures 1A and 1B). The density distribution of the quantitative values after logarithmic transformation showed a significant normal distribution between −10 and 10, which is in line with the expectation of the whole protein quantitative theory (Figure 1C). In this scenario, 3,957 and 3,450 proteins were identified, respectively, in *T. brucei* and *T. evansi*, and 2,123 proteins were shared between the two species (Figure 1D and Table S1). Differentially expressed proteins were further categorized into groups presented by Tb-exclusive, Te-exclusive, Common and Tb-high, and Common and Te-high (corresponding to Tb-e, Te-e, Tb-h, and Te-h in the figures and figure legends, respectively). Species-exclusive proteins were identified in three replicates of one species and in none in the other species; the latter two groups were defined by fold change >2 and p value <0.05 (Table S2). The numbers of the proteins categorized in the four groups were 555, 272, 516, and 369 (Table S2), respectively. These four groups of proteins were consistently the most abundant in the nucleus; the next most prevalent localization for these proteins was the cytoplasm (Figure 1E). More than 80% of the differentially expressed proteins that regulate cell motility such as the dynein complexes and that are associated with flagellum (synonymous to cilium) organization and movement (Langousis and Hill, 2014) were up-regulated in *T. evansi*, whereas proteins with oxidoreductase activity and the zinc finger-type RBPs were more prevalent in *T. brucei*

A

PTM type	Peptides		Modified peptides		Modified proteins		Modified sites	
	T. b	*T. e*	*T. b*	*T. e*	*T. b*	*T. e*	*T. b*	*T. e*
Ac	8653	6647	7401	4931	2533	1942	7445	4965
Cr	13699	11087	11861	9494	3162	2729	12024	9608
Hib	12384	10800	11101	9809	2643	2655	11129	9851
Ma	5852	4658	225	110	128	65	231	112
Su	4918	4009	1233	253	384	99	1242	257
Ub	3835	2950	981	549	462	270	999	556
Me3	406	349	49	42	42	39	56	46
Ph	12885	10575	7722	6256	2520	2395	8351	6739
Og	4551	6209	15	33	15	33	16	46
Ng	10188	9642	1051	795	602	470	1163	860

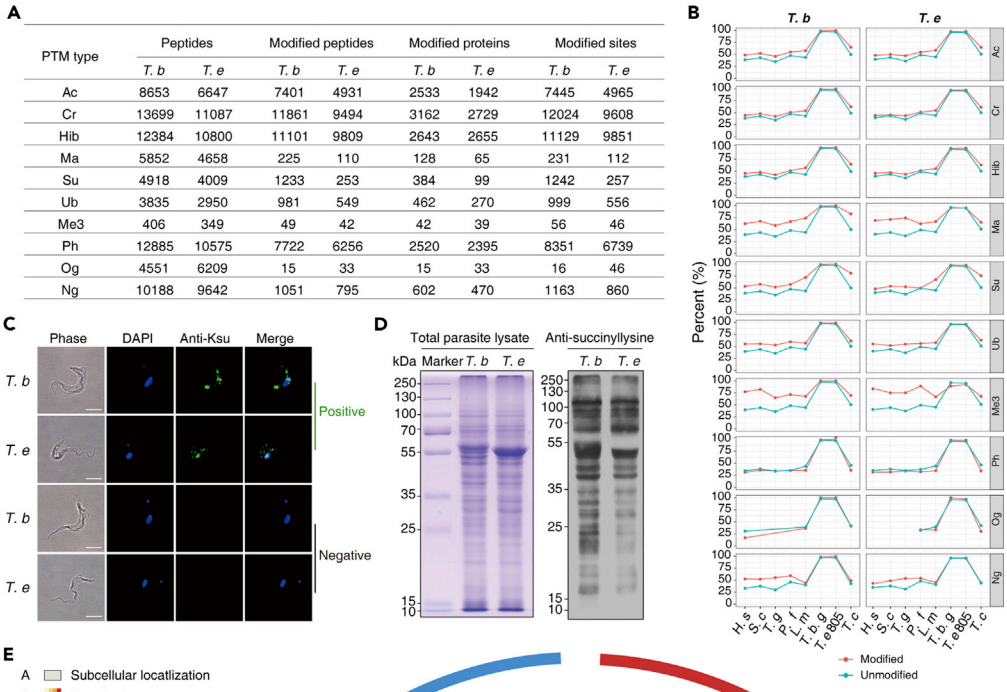

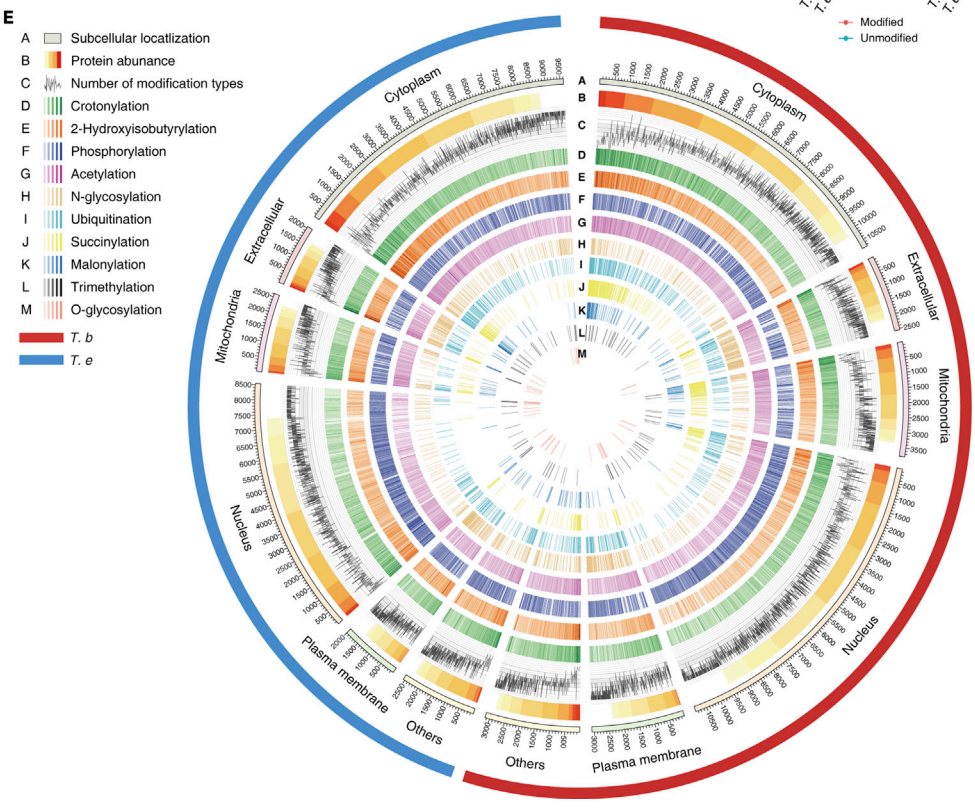

Figure 2. In-Depth Global Identification Highlights Species-Specific PTMs

(A) Summary of the identified proteins and PTM sites.

(B) Analysis of the modified sites in *T. brucei* and *T. evansi* with their respective orthologs in *Homo sapiens*, *S. cerevisiae*, *Toxoplasma gondii*, *Plasmodium falciparum*, and other species of trypanosomatid parasites. Sites were deemed to be phylogenetically conserved when the amino acids of the homologous proteins were identical following alignment. Percentages of conserved modified and unmodified sites are shown in red and blue, respectively.

Figure 2. *Continued*

(C) Immunofluorescent staining of methanol-fixed *T. brucei* and *T. evansi* with the anti-succinyl lysine antibody (green). Nuclei are stained with DAPI (blue). Pan anti-succinyl lysine antibody (positive) and normal mouse IgG (negative control) were added as the primary antibody. Scale bar, 10 μm.

(D) Coomassie blue staining of 20 μg BSF trypanosome lysates showed equal loading amounts. Western blot probed with a monoclonal anti-succinyl lysine antibody.

(E) Protein abundance and PTMs in each subcellular structure. The outermost colors represent different subcellular structures, and the color gradient indicates the abundance of each protein. The number of PTM types that can occur on the proteins is represented by the line chart, whereas the numbers of modified sites of different types are illustrated by various color gradients. Ph, phosphorylation; Ac, acetylation; Cr, crotonylation; Hib, 2-hydroxyisobutyrylation; Ma, malonylation; Su, succinylation; Ub, ubiquitination; Me3, trimethylation.

See also Figure S2 and Tables S1, S2, and S3.

than in *T. evansi* (Figure 1D and Table S3). Tb-exclusive and Tb-high expressed proteins were predominantly enriched in the citrate cycle (TCA cycle) pathway (Figures 1D and 1F and Table S3).

To validate the differential expression of proteins in these two parasites, parallel reaction monitoring was applied to quantify individual unique peptides. Targeted verifications were performed on 13 differentially expressed proteins, and the regulatory trends of these proteins in both parasites were consistent with the proteome results (Figure S1 and Table S2).

In-Depth Global Identification Highlights Species-Specific PTMs

A proteomic repertoire of 10 types of PTMs was generated following PTM-specific affinity-enrichment techniques that facilitate the detection of transient and substoichiometric PTMs (Figures 1A, 2A, and S2A–S2C and Table S1 and Data S1). The replicates of the same experiments clustered tightly in PCA (Figure S2A), and the distribution of the quantitative values after logarithmic transformation was reasonable (Figures S2B and S2C). Specific masses of the modified peptides were matched to the corresponding proteins to count the modification sites. There were 42,656 and 33,040 modified sites identified in 10 PTM-omics of *T. brucei* and *T. evansi*, respectively (Figure 2A and Table S1). Respective PTM map and regulatory networks of the proteins identified from the two trypanosome species were accomplished. In general, modified sites were more conserved when aligned with their respective orthologs in species of trypanosomatid parasites, highlighting the functional significance of these sites (Figure 2B). The most significant difference in PTMs between the two species was succinylation, which predominantly occurred in *T. brucei* (Figures 2A, 2C and 2D). A circular proteome map was constructed to further depict the similarities and differences between the proteins and PTMs of the two parasites; the modified proteins were relatively broadly distributed in multiple cellular compartments, and the distribution of modified proteins was much prevalent across the cytoplasm (Figures 2E and S2D). There is no obvious linear relationship between the level of phosphorylation and protein abundance, and the phosphosites were not highly conserved, indicating that protein phosphorylation is more extensive than other PTM types (Figures 2B and 2E).

Functionally, PTMs were significantly involved in pervasive biological processes including signal transduction, translation, RNA processing, transport, and protein turnover in the parasites (Figure S2E and Table S3). In both *T. brucei* and *T. evansi*, a large number of thioredoxins and the 70-kDa heat shock proteins (HSP70s) were significantly succinylated, but it was malonylated exclusively in *T. brucei* (Table S3). The involvement of PTMs in oxidation-reduction seems to be more critical to *T. brucei* (Table S3).

Furthermore, similar to the aforementioned proteomic analysis, all differentially modified proteins were classified into four groups, and the modification site numbers of these four groups were 1547, 809, 2201, and 2024, respectively (Table S2). We observed that the differentially modified proteins were predominantly involved in carbon metabolism and translation, and the non-overlap proteins for malonylation in *T. brucei* and *T. evansi* still share some significant pathways, especially in relation to carbohydrate metabolism (Figure S3A). In addition, an interactive network of all differentially modified proteins was constructed (Figure S3B). These proteins were predominantly involved in cellular processes such as translation, glycolysis, and ubiquitin-mediated protein degradation. An inosine-5′-monophosphate dehydrogenase (IMPDH1, Tb927.10.16120), which catalyzes the conversion of inosine-5′-monophosphate to xanthosine-5′-phosphate, the major pathway in purine metabolism (Bessho et al., 2013), exhibited extremely strong interactions with other proteins.

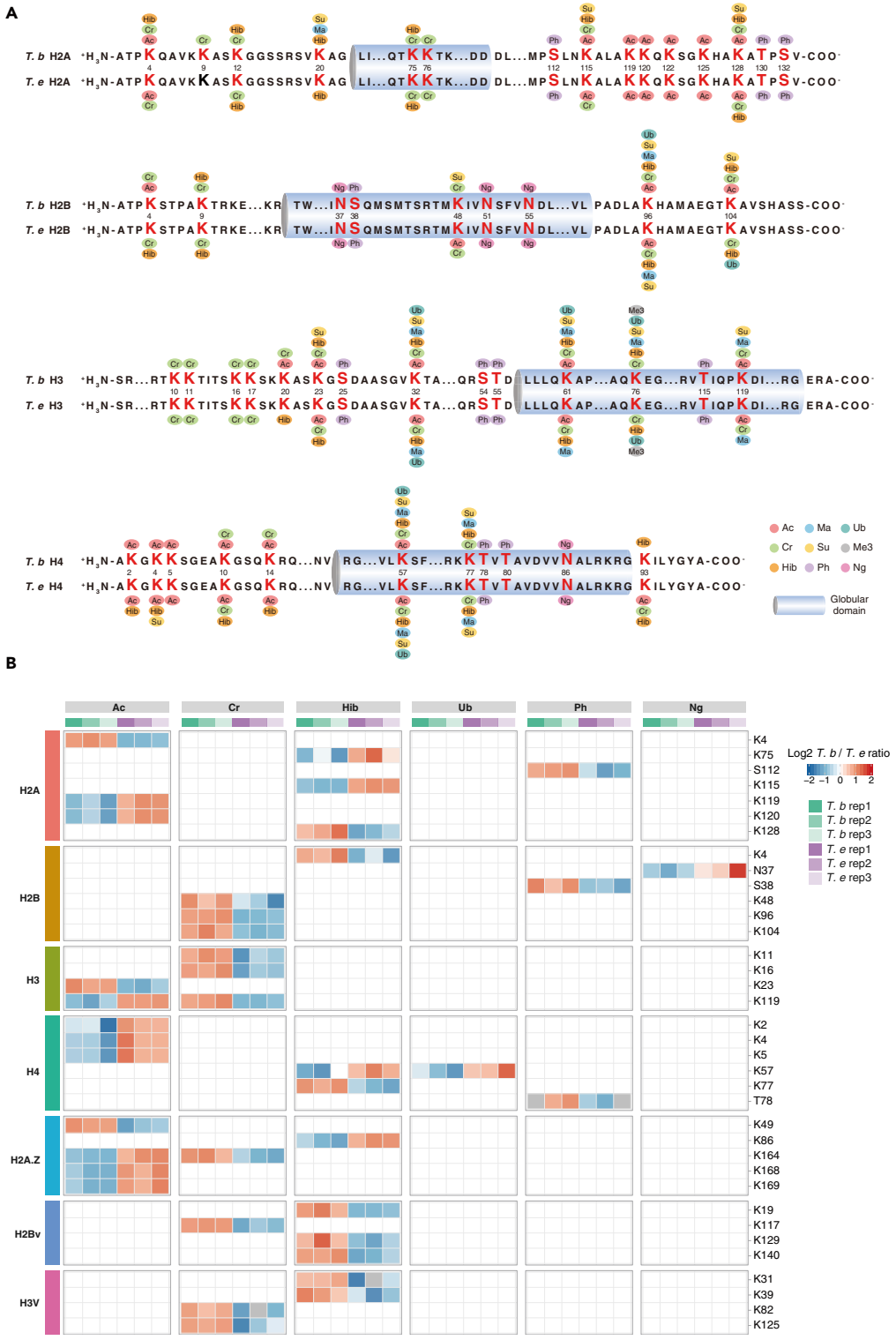

Figure 3. Histone Modifications Are Highly Conserved in African Trypanosomes

(A) PTMs of canonical histones of both *T. brucei* and *T. evansi*. Cylinders indicate the globular domain of histones. Sequences of mature histones are shown with the modified residues in bold (the numbers represent the amino acid position following removal of the initial methionine).

(B) Heatmap displaying the significance (log2 *T. b*/*T. e* ratio) of all modified sites on histones and their variants.

See also Figure S4 and Table S4.

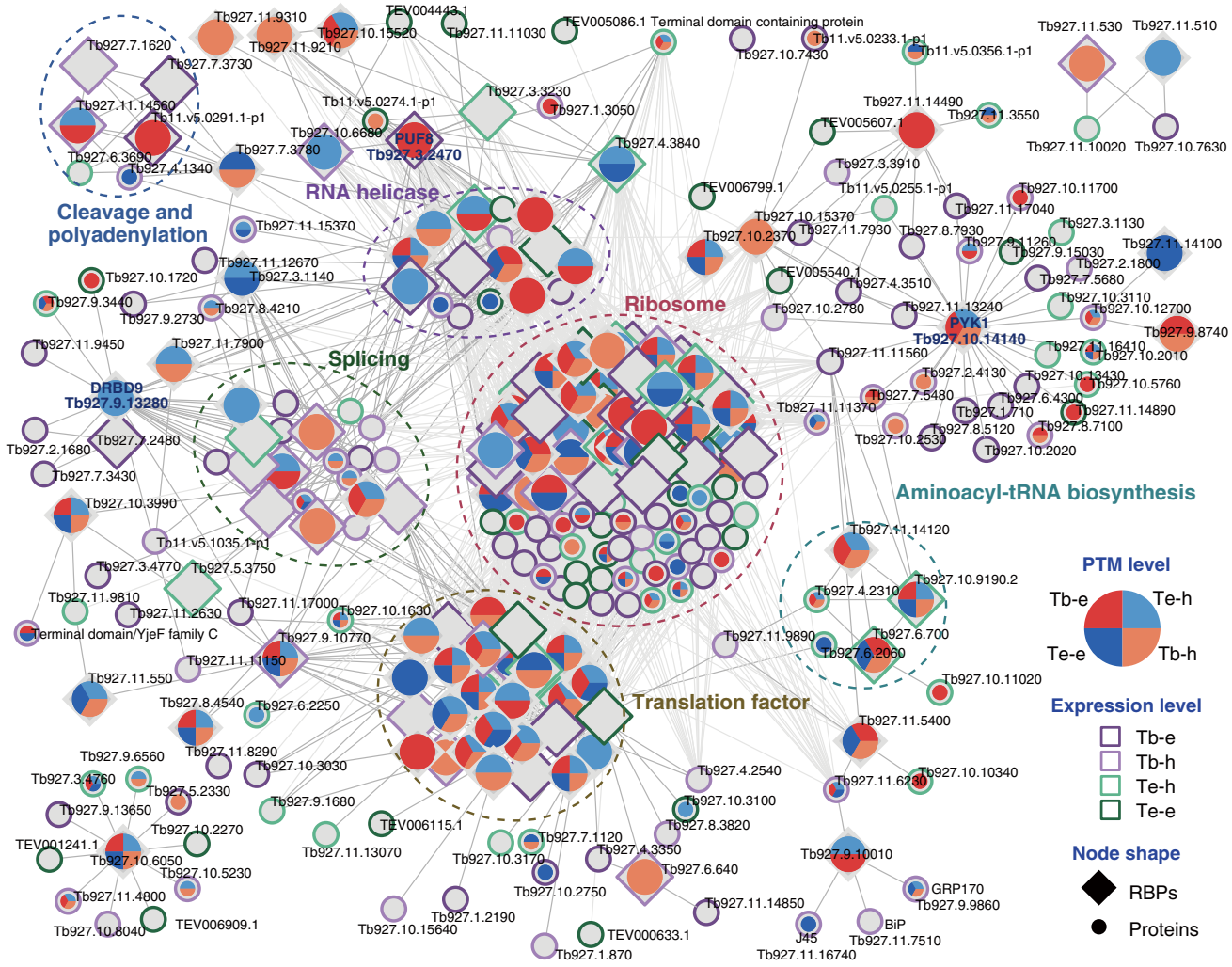

Figure 4. PTMs and Their Association with Networks of RNA-Binding Proteins (RBPs)

A map of protein-protein interaction networks for RBPs (square) and their substrate proteins (circle). The interactive proteins were connected by lines; different border colors represent the regulation types of protein expression level, and the filling colors represent the trends of PTMs that occur on this protein.

Histone Modifications Are Highly Conserved in African Trypanosomes

A large number of histone marks were observed (Figure 3A and Table S4). A total of 162 histone marks were identified in *T. brucei*, 135 of which were novel, whereas all the 134 marks in *T. evansi* were reported for the first time. Furthermore, 119 histone marks were shared in the two parasites.

An extensive range of PTMs occurred on the tails of histones compared with the globular domains. In general, variant histones are less conserved than canonical histones (Croken et al., 2012). However, the modified sites of the variant histones were extensively similar between the two parasites (Figure S4). Remarkably, several hyper-acetylated regions that have been postulated as being important in the establishment of euchromatins and the regulation of particular gene clusters under particular circumstances were identified. H2A.Z was predominantly regulated by hyperacetylation, with K49 in the N terminus exhibiting greater levels of acetylation in *Tb*H2A.Z. Conversely, K164, K168, and K169 in the C terminus exhibited greater levels of acetylation in *Te*H2A.Z (Figure 3B and Table S4). Hyperacetylated regions at the C terminus of histone H2A and the N terminus of histone H4 were predominant in *T. evansi*. Furthermore, many residues underwent multiple PTMs and had similar or opposite effects on chromatin structure at different times; modification on H2BK96, H3K32, H3K61, H3K76, and H4K57 exhibited the most prominent effects in this regard.

RNA-Binding Proteins, the Regulatory Elements of Gene Expression in Trypanosomes, Undergo Extensive PTMs

The absence of RNAP II promoters in trypanosomes greatly simplifies the task of elucidating the contribution of RBPs to global gene regulation. A regulatory network of differentially expressed or modified RBPs and associated interacting proteins was constructed (Figure S5). The identified RBPs were predominantly involved in RNA processing, splicing, and ribosome biogenesis. Pyruvate kinase 1 (PYK1, TritrypDB: Tb927.10.14140), a rate-limiting enzyme involved in the glycolysis pathway, also exhibited RNA-binding activity (Lueong et al., 2016), was differentially regulated by six PTMs in the two trypanosomes. Pumilio homology domain family member 8 (PUF8, TritrypDB: Tb927.3.2470), which has been implicated in various aspects of ribosomal RNA metabolism (Droll et al., 2010), was specifically acetylated in *T. brucei* and closely related to RNA helicase. Furthermore, the double RNA-binding domain protein 9 (DRBD9, TritrypDB: Tb927.9.13280) with K144hib, which is predominantly present in *T. evansi*, appears to be highly correlated with splicing proteins.

Kinase-Phosphosite Regulatory Networks Highlighted Key Factors in Differential Phosphorylation

The sequence contexts that underwent phosphorylation in both *T. brucei* and *T. evansi* were analyzed. The flanking sequences of phosphosites exhibited different trends in the two trypanosomal species, suggesting that protein kinases act specifically (Figures 5A and 5B and Table S5). Most of the motifs in which the arginine (R) was present at the −2 or −3 position of the modified serine (S) were enriched in CAMK and AGC kinases. Notably, most CMGC kinases, chiefly CDK, MAPK, DYRK, and GSK with proline (P) at the +1 position, always had higher levels of phosphorylation in *T. brucei*. In *T. evansi*, acidic amino acids (aspartic acid [D] or glutamic acid [E]) occurred more frequently at the +1 position of phosphosites; most of the TAF1 and CMGC/CK2 kinases contained such phosphorylation motifs.

The potential regulatory relationships between the differential expression and autophosphorylation of kinases with their substrate phosphosites were also predicted in this study; both factors were closely related to the phosphorylation level of whole proteins (Figures 5C and 5D). The elevated expression of cdc2-related kinase 6 (CRK6, TritrypDB: Tb927.11.1180) and the elevated autophosphorylation of tyrosine 34 (Y34) of CRK3 (TritrypDB: Tb927.10.4990) in *T. brucei* affected the phosphorylation level of other proteins, and Y34 was located at the ATP-binding sites (Figure 5E and Video S1); these were key factors leading to the differential phosphorylation of *T. brucei* and *T. evansi*.

Variation in the PTM-omes of Flagellar Proteins Reflected the Differences in Parasite Motility

The trypanosome flagellum contains a canonical 9 + 2 microtubular axoneme alongside which the paraflagellar rod (PFR) runs (Bastin et al., 1998). The axoneme emanates from the basal body through the transition zone and is laterally connected to the cell membrane via the flagellum attachment zone (FAZ) (Figure 6). In each part of the flagellum, a majority of the proteins were highly or exclusively modified in *T. evansi* (Figure 6 and Table S6). Moreover, the differential PTMs associated with these proteins further explains the more flexible appearance of *T. evansi* (Bargul et al., 2016) (Tables S3 and S6). The inner-arm dynein (IAD5-1, TritrypDB: Tb927.7.920), knockdown of which causes cell motility defects, was highly expressed in *T. evansi* (Wei et al., 2014). K1,134 of IAD5-1 was acetylated exclusively in *T. brucei* and 2-hydroxyisobutyrylated in *T. evansi*. The flagellum attachment zone protein 2 (FAZ2, TritrypDB: Tb927.1.4310) was heavily phosphorylated, and a similar observation was reported in *T. brucei* (Nett et al., 2009b). However, the phosphorylation on this protein was more prevalent in *T. evansi*. *N*-glycosylated sites were mainly identified in two proteins, PFR component (PFC16, TritrypDB: Tb927.10.11300) and flagellum adhesion protein 2 (FLA2, TritrypDB: Tb927.8.4060), and the modifications occurred more frequently in *T. brucei*.

PTMs Regulated Energy Metabolism and Trypanosomatid-Specific Redox System

Eight PTMs were significantly enriched in the glycolysis pathway (Figure S3), which is the main energy metabolism pathway in BSF trypanosomes (Haanstra et al., 2016). The subcellular localization profiles of glycolytic enzymes of both *T. evansi* and *T. brucei* were similar (Moreno and Nava, 2015), and most enzymes had multiple modifications (Figure 7A). Notably, the acetylation and 2-hydroxyisobutyrylation that occurred on the three rate-limiting enzymes were highly prevalent in *T. evansi* (Figure S5). Furthermore, it was observed that many PTMs occurred at key residues of the enzymes. For example, the K117 of fructose-1,6-

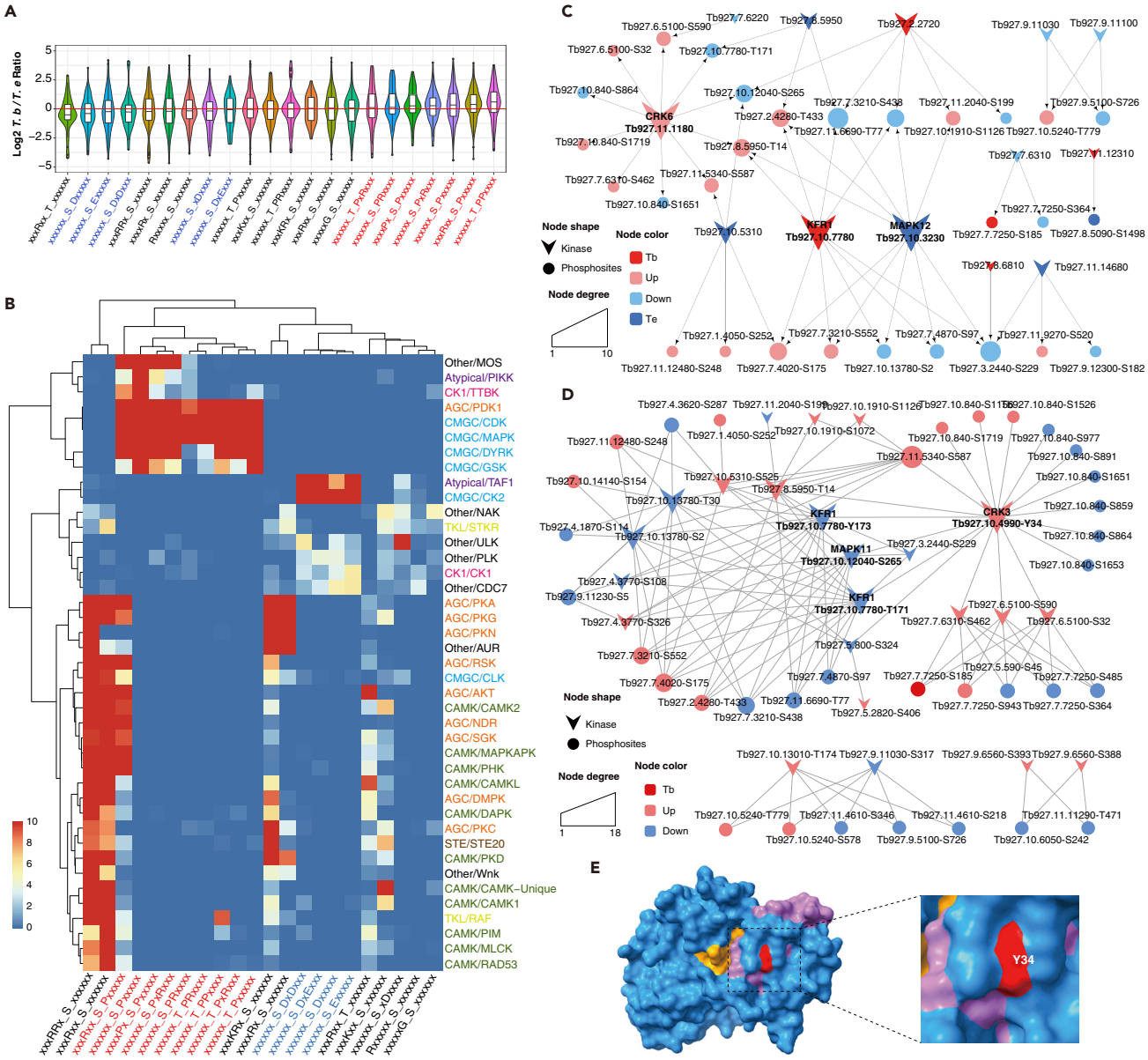

Figure 5. Kinase-Phosphosite Regulatory Networks Highlighted Key Factors in Differential Phosphorylation

(A) Violin plot analysis comparing the phosphorylation levels and distributions of different sequence motifs in the two parasites. The vertical position of each histogram represents the relative modified level of *T. brucei* and *T. evansi*.

(B) Heatmap displaying the significance of the correlation of kinase types and motifs. The gradient color represents the degree of enrichment (log10 p value) of the motif in the corresponding kinase.

(C and D) The regulatory relationship between differentially expressed (C) and autophosphorylated (D) kinases with their substrate phosphosites. The arrows represent differentially expressed kinases, and circles represent phosphorylated sites. The size of each node reflects the degree within the network. The colors of the nodes reflect the types of regulation.

(E) Differential phosphorylated sites detected in CRK3 are represented by the three-dimensional structure of protein. The phosphosite is shown in red, and the ATP-binding pocket and active sites are marked in purple and yellow, respectively (PDB: 4GCJ).

See also Table S5 and Video S1.

bisphosphate aldolase (ALDO), which could be modified by six types of PTMs, is precisely positioned at the active site (Figure 7B, Video S2), and N338 of enolase (ENO), which was *N*-glycosylated, is located near the substrate-binding pocket and metal-binding sites (Figure 7B, Video S3).

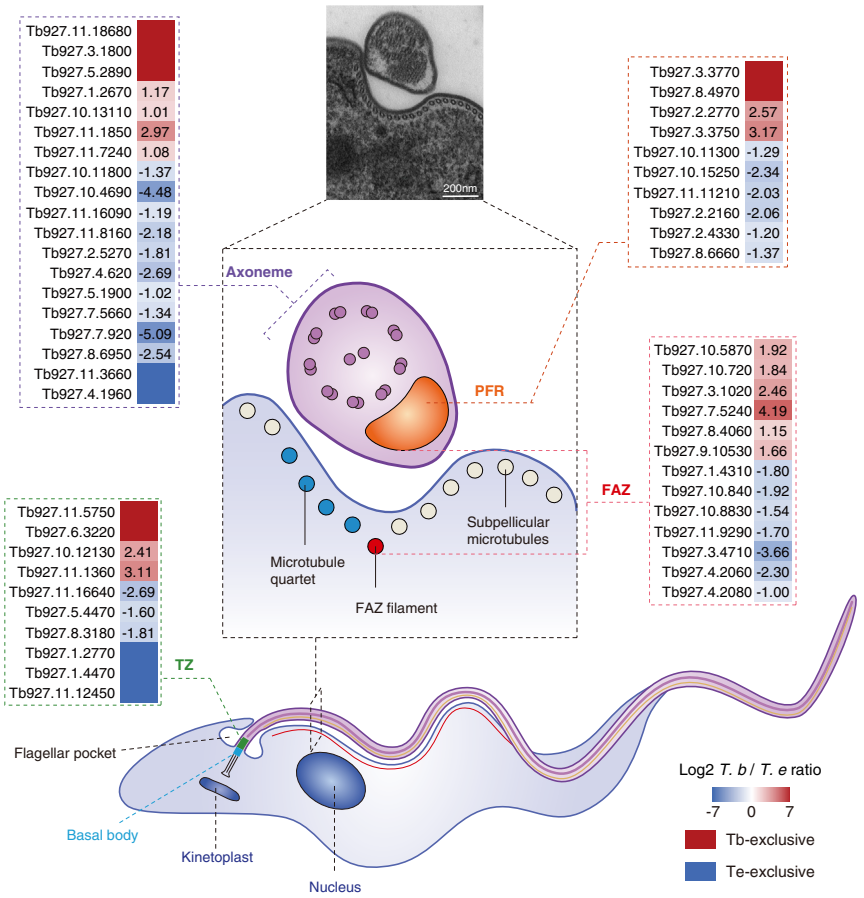

Figure 6. Differences in the PTM-omes of Flagellar Proteins Associated with Parasite Motility

A simplified schematic diagram shows the architecture of the trypanosome flagellum, and the transmission electron microscopic image shows a transverse section of the flagellum. Scale bar, 200 nm. Heatmaps displaying the differential expression levels of proteins in each part of the two trypanosomes. See also Table S6.

Trypanosomes, as early branching eukaryotes, have evolved in a manner that has resulted in a unique trypanothione-based thiol-redox system (Manta et al., 2013). Trypanothione reductase (TryR, TritrypDB: Tb927.10.10390), which has been considered as a target for antitrypanosomatid drugs, recycles trypanothione disulfide (TS_2) back to dihydro-trypanothione ($T(SH)_2$), and tryparedoxin (TXN) catalyzes the electron transferred from $T(SH)_2$ to different protein targets that are normally involved in multiple functions such as cell proliferation and antioxidant defense (De Gasparo et al., 2019). We observed multiple PTMs pertaining to TryS, TryR, and TXN, and both TXN1 and TXN2 were expressed more prevalently in *T. brucei* than *T. evansi* (Figure 7 and Table S7).

Crosstalk between Different Types of PTMs Involved in Critical Biological Processes

Correlation and Functional Overlaps

Proteins and sites modified by different PTMs were compared to assess the significance of the overlaps (Figure S6A and Table S8). A large amount of overlap was observed among acetylated, crotonylated, and 2-hydroxyisobutyrylated proteins in both *T. brucei* and *T. evansi*. The succinylated sites in *T. brucei* had higher correlations with other lysine (Lys)-modified sites. However, in *T. evansi*, these sites had a more significant correlation with malonylated sites. Functionally, most of these PTMs were positively associated with carbohydrate metabolism (Figure S6B). For the disulfide isomerases, *N*-glycosylation was significantly enriched and negatively correlated with other PTMs.

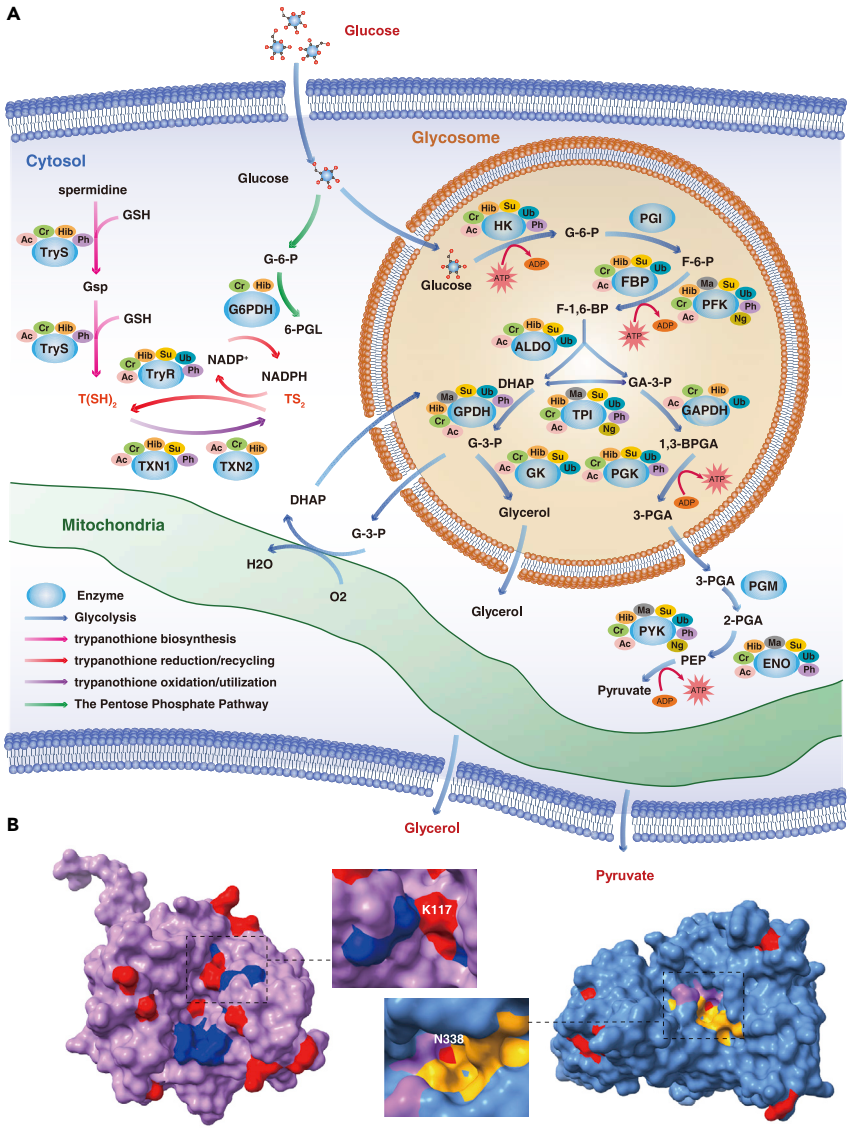

Figure 7. PTMs Regulate Energy Metabolism and Trypanosomatid-Specific Redox System

(A) Schematic diagram of the glycolysis pathway and trypanothione-based thiol-redox system in trypanosomes. Glycerol 3-phosphate (G3P) is reoxidized by the mitochondrial glycerol phosphate complex and returned to the glycosome for further cycling. The consumption of NADPH by trypanothione reductase results in the maintenance of trypanothione in a reduced state; the latter protein is generated by the pentose phosphate pathway. G-6-P, glucose 6-phosphate; F-6-P, fructose 6-phosphate; F-1,6-BP, fructose 1,6-bisphosphate; DHAP, dihydroxyacetone phosphate; GA-3-P, glyceraldehyde 3-phosphate; G-3-P, glycerol-3-phosphate; 1,3-BPGA, 1,3-bisphosphoglycerate; 3-PGA, 3-phosphoglycerate; 2-PGA, 2-phosphoglycerate; PEP, phosphoenolpyruvate; 6-PGL, 6-phosphogluconolactone; GSH, reduced glutathione; Gsp, mono-glutathionylspermidine; TS_2, trypanothione disulfide; $T(SH)_2$, dihydro-trypanothione; HK, hexokinase; PGI, glucose phosphate isomerase; PFK, phosphofructokinase; TPI, triosephosphate isomerase; GPDH, glycerol-3-phosphate dehydrogenase; GK, glycerol kinase; GAPDH, glyceraldehyde-3-phosphate dehydrogenase; PGK, phosphoglycerate kinase; PGM, phosphoglycerate mutase; PYK, pyruvate kinase; G6PDH, glucose-6-phosphate dehydrogenase; TryS, trypanothione synthetase; TryR, trypanothione reductase; TXN, tryparedoxin.

(B) Differentially modified sites detected in ALDO (left panel) and ENO (right panel) are represented by the three-dimensional structure of proteins. The modified sites are shown in red, and the active sites of ALDO are marked in blue. The substrate-binding pocket and the metal-binding sites of ENO are marked in yellow and purple, respectively. Protein structures were obtained from the Protein DataBank (PDB, ALDO: 1F2J, ENO: 1OEP).

See also Figure S5, Videos S2 and S3.

Lysine Acylations

Lys can be modified by various PTMs, especially acylations (Sabari et al., 2017). In this study, five types of Lys-acylated proteins were quantified and the structural differences among their chains were observed. Quantitative correlations between different PTMs occurring on Lys were predicted based on the Pearson correlation coefficient (Figure S6C). In addition to succinylation, Lys malonylation was negatively correlated with other acylations.

DISCUSSION

PTMs significantly increase the diversity and complexity of the proteome by altering protein function, localization, and protein-protein interactions. Previous research indicated that the expression and function of the surface-variant glycoproteins of *T. brucei* were controlled by several ubiquitylation pathways (Zoltner et al., 2015). Nett et al. used sequential strong-cation exchange and TiO_2 enrichment of BSF *T. brucei* phosphopeptides, identified 1,204 phosphorylation sites on 491 proteins (Nett et al., 2009b), and employed anti-phosphotyrosine antibodies to identify 34 phosphotyrosine sites in PCF *T. brucei* (Nett et al., 2009a). Using stable isotope labeling by amino acids in cell culture, another study reported stage-specific phosphorylation changes in *T. brucei* and showed that differential phosphorylation is widespread between the PCF and BSF (Urbaniak et al., 2013). Recent works detected 288 Lys acetylation sites in 210 proteins of PCF and 380 sites in 285 proteins of BSF; notably, most K-ac proteins are enriched in metabolic processes, suggesting that they are essential for parasite adaptation in the hosts (Moretti et al., 2018). However, so far, these studies are not comprehensive with focus on a few PTMs, and such study on *T. evansi* has not been reported.

In this study, we systematically investigated and compared the features of PTMs in the BSF of *T. brucei* and *T. evansi*. We observed that succinylation occurred most differentially between the two trypanosomes (Figures 1A–1C). Many studies have shown that succinylation played an important role in the metabolic regulation, especially in the mitochondrial pathway (Yang and Gibson, 2019). The higher level of protein succinylation in *T. brucei* may explain the metabolic differences between *T. brucei* and *T. evansi*. The most abundant PTMs in the two trypanosome species were crotonylation, 2-hydroxyisobutyrylation, acetylation, and phosphorylation, and fewer *O*-GlcNAcylated and trimethylated proteins were identified (Figure 1A). The number of *O*-GlcNAcylated proteins in the two species is similar to that identified in the *Plasmodium* and *Toxoplasma* parasites (Aquino-Gil et al., 2018; Kupferschmid et al., 2017).

Proteins exhibiting species-specific expression and modification were revealed. Among the protein activities that were analyzed, oxidoreduction, which is functionally linked to environmental adaptation, was highly expressed and modified in *T. brucei* (Figure 1D and Table S7). This result correlates well with findings in *Plasmodium*, where antioxidant proteins were preferentially expressed in the mosquito stage of the parasite (Wang et al., 2018). Obviously, the modifications are essential in promoting the function of the antioxidant proteins in the insect vectors. In addition, the dynein complex and proteins associated with flagellar movement that supported the flexible appearance of *T. evansi* were predominantly expressed and modified (Figure 1D and Table S6). Furthermore, *N*-glycosylation occurred more frequently in flagellar proteins of *T. brucei*, suggesting that this PTM may be detrimental to parasitic motility. These findings might explain why *T. evansi* has a more flexible appearance with greater adaptability in relation to movement in restricted environments compared with *T. brucei* (Bargul et al., 2016; Broadhead et al., 2006; Langousis and Hill, 2014). Notably, IMPDH1, which exhibited extremely strong interactions with other proteins (Figure S3B), has been shown to be essential for the survival of *T. brucei*. It differs in structure from its mammalian counterpart and therefore may represent a novel anti-trypanosomal drug target (Bessho et al., 2013).

The enrichment of Tb-exclusive and Tb-high expressed (Figure 1F) and modified (Figure S3A) proteins in the citrate cycle may indicate that, after the parasitemia has reached a certain point, the parasite began to switch from slender form to stumpy form, a process that is regulated by QS signaling pathways (Mony et al., 2014); it is likely that proteins participating in the tricarboxylic acid cycle are expressed to prepare for development in the insect vector and for the maintenance of well-developed mitochondria with abundant cristae (Haanstra et al., 2016).

Although unusually divergent from other eukaryotes, trypanosomal parasites have kept a conserved feature in their histones (Picchi et al., 2017). The protein sequences of histones of *Trypanosoma* parasites

and other eukaryotes differ greatly but are compacted in a similar chromatin structure and organization (Croken et al., 2012; Picchi et al., 2017). The histones and their PTMs were well conserved in trypanosomes, and 88.8% of the histone marks in *T. evansi* are also present in *T. brucei* (Figure 3 and Figure S4). Most modified sites on histones of *T. brucei* have been characterized in previous studies, such as H4K4ac, which is cell cycle regulated and mediated by histone acetyltransferase 3 in *T. brucei* (Siegel et al., 2008), and H4K10 is likely acetylated in all nucleosomes at transcription start sites (Kawahara et al., 2008; Siegel et al., 2009). Previous study found that deacetylation of H4K14ac and replacing H4K10ac by arginines delayed DNA replication and reduced transcription in *Trypanosoma cruzi* (Ramos et al., 2015), and both H4K10ac and H4K14ac were also identified in our study (Croken et al., 2012; Picchi et al., 2017). Dimethylation and trimethylation of H3K76, activities that are regulated by DOT1A and DOT1B, were observed in both parasites (Picchi et al., 2017). Hyperacetylation occurred in different histone regions of *T. brucei* and *T. evansi*, which suggested that the acetylated sites in each hyperacetylated region may always be co-regulated and that each hyperacetylated region has distinct functions depending on its position. In addition, a large number of novel histone modifications were revealed for the first time, laying the foundation for further research. Many PTMs on histones are substoichiometric, reflecting the dynamic properties of chromatin. The diversity of histone PTMs in trypanosomes reveals a dynamic role in the regulation of histone function.

The regulation of RNA metabolism is another important basis for determining cell function and fate. At the protein expression level, the higher expression of zinc finger-type RBPs in *T. brucei* compared with that of *T. evansi* is in accordance with the finding that there are a greater number of genes in *T. brucei* than in *T. evansi* (Figure 1D) (Zheng et al., 2019). Furthermore, dynamic modifications of RBPs add another layer of gene regulation. RBPs in trypanosomes execute important role in regulating mRNA abundance and translational repression in combination with precursor mRNA or a portion of mature mRNA. Although there is no significant difference in the expression level of the rate-limiting enzyme in the glycolysis pathway, a variation in PTMs in PYK1, a protein that was also an RBP, is likely to affect the expression of other proteins in various metabolic processes (Figure 4). Specific expression and modification of PUF8 in *T. brucei* might indicate different mechanisms of rRNA maturation in the two trypanosomal parasites (Figure 4).

Furthermore, both CRK3 and CRK6 are essential in regulating the cell cycle and differentiation in *T. brucei* (Jones et al., 2014), and Y34 of CRK3 was located at the ATP-binding sites, which are the targets of most kinase inhibitor-based drugs (Figure 5). This provides support for the concept that trypanosome-specific inhibitors can be developed. Furthermore, a notable observation is that most glycolytic enzymes that regulate the main energy-providing pathway of BSF trypanosomes were modified, and some of the modified sites were in close proximity to the catalytic sites of these enzymes, suggesting that PTMs critically modulate the activity of key enzymes. Critical enzymes with "Erasers" and "Writers" function in the modification processes are targets for drug development and some inhibitors have already entered the market in the treatment of cancer and neurological diseases (Arrowsmith et al., 2012). The existing drugs for trypanosomiasis lead to side effects, and drug-resistant trypanosomes are emerging, emphasizing the need for action to discover novel effective trypanocidal drugs to address unmet pharmaceutical needs (Field et al., 2017). How to quickly discover the drugs and develop them effectively has always been a difficult point in the prevention and treatment of trypanosomiasis. We present evidence that sirtuins can be potential targets for the therapy for trypanosomiasis, as these enzymes are important factors controlling growth and differentiation during infection.

In conclusion, our study has revealed the most comprehensive PTMomics in the two African trypanosomal parasites, *T. brucei* and *T. evansi*. The discoveries of parasite-specific modifications, especially the fine locations of the modified residues in the metabolic enzymes of both *T. brucei* and *T. evansi*, lay the foundation for the development of new drugs.

LIMITATIONS OF THE STUDY

The values of PTM intensity were not normalized by protein intensity. We have compared the PTM data with or without normalization to that of the proteomic data. There was no significant correlation between the PTM level and the protein expression level before normalization. After normalization, however, the PTM values were negatively affected by the changes in protein levels, but should not be interpreted as real modification changes.

METHODS

All methods can be found in the accompanying Transparent Methods supplemental file.

DATA AND CODE AVAILABILITY

All data is available in the main text or the Supplemental Information. The MS spectrometry measurement files have been deposited at the ProteomeXchange consortium (http://proteomecentral.proteomexchange.org) via PRIDE Archive (PXD016245).

SUPPLEMENTAL INFORMATION

Supplemental Information can be found online at https://doi.org/10.1016/j.isci.2020.101074.

ACKNOWLEDGMENTS

We appreciate very much the kind assistance from PTM BioLab scientists in the omic analysis. This study was supported by the Distinguished Scientist grant from Shenyang Agricultural University and Liaoning Province [8804-880416076], and CAMS Innovation Fund for Medical Sciences (CIFMS) [2019-I2M-5-042].

AUTHOR CONTRIBUTIONS

N.Z. performed most of the experiments, analyzed the data, and wrote the first draft of the manuscript. N.J. mentored the experiments, K.Z., L.Z., D.Z., and X.S. assisted parasite purification, Y.F. and R.C. performed the immunofluorescent experiment, N.Y. and Z.C. assisted bioinformatics analysis, X.S. provided *T. evansi* isolates, Z.L. provided *T. brucei* strains, Q.C. conceived the study, analyzed the data, and finalized the manuscript.

DECLARATION OF INTERESTS

The authors declared no competing interests.

Received: January 7, 2020
Revised: February 22, 2020
Accepted: April 14, 2020
Published: May 22, 2020

REFERENCES

Aquino-Gil, M.O., Kupferschmid, M., Shams-Eldin, H., Schmidt, J., Yamakawa, N., Mortuaire, M., Krzewinski, F., Hardiville, S., Zenteno, E., Rolando, C., et al. (2018). Apart from rhoptries, identification of *Toxoplasma gondii*'s O-GlcNAcylated proteins reinforces the universality of the O-GlcNAcome. Front. Endocrinol. *9*, 450.

Arrowsmith, C.H., Bountra, C., Fish, P.V., Lee, K., and Schapira, M. (2012). Epigenetic protein families: a new frontier for drug discovery. Nat. Rev. Drug Discov. *11*, 384–400.

Bargul, J.L., Jung, J., McOdimba, F.A., Omogo, C.O., Adung'a, V.O., Kruger, T., Masiga, D.K., and Engstler, M. (2016). Species-specific adaptations of trypanosome morphology and motility to the mammalian host. PLoS Pathog. *12*, e1005448.

Bastin, P., Sherwin, T., and Gull, K. (1998). Paraflagellar rod is vital for trypanosome motility. Nature *391*, 548.

Berriman, M., Ghedin, E., Hertz-Fowler, C., Blandin, G., Renauld, H., Bartholomeu, D.C., Lennard, N.J., Caler, E., Hamlin, N.E., Haas, B., et al. (2005). The genome of the African trypanosome *Trypanosoma brucei*. Science *309*, 416–422.

Bessho, T., Morii, S., Kusumoto, T., Shinohara, T., Noda, M., Uchiyama, S., Shuto, S., Nishimura, S., Djikeng, A., Duszenko, M., et al. (2013). Characterization of the novel *Trypanosoma brucei* inosine 5'-monophosphate dehydrogenase. Parasitology *140*, 735–745.

Broadhead, R., Dawe, H.R., Farr, H., Griffiths, S., Hart, S.R., Portman, N., Shaw, M.K., Ginger, M.L., Gaskell, S.J., McKean, P.G., et al. (2006). Flagellar motility is required for the viability of the bloodstream trypanosome. Nature *440*, 224–227.

Buscher, P., Cecchi, G., Jamonneau, V., and Priotto, G. (2017). Human African trypanosomiasis. Lancet *390*, 2397–2409.

Carnes, J., Anupama, A., Balmer, O., Jackson, A., Lewis, M., Brown, R., Cestari, I., Desquesnes, M., Gendrin, C., Hertz-Fowler, C., et al. (2015). Genome and phylogenetic analyses of *Trypanosoma evansi* reveal extensive similarity to *T. brucei* and multiple independent origins for dyskinetoplasty. PLoS Negl. Trop. Dis. *9*, e3404.

Cayla, M., Rojas, F., Silvester, E., Venter, F., and Matthews, K.R. (2019). African trypanosomes. Parasit. Vectors *12*, 190.

Croken, M.M., Nardelli, S.C., and Kim, K. (2012). Chromatin modifications, epigenetics, and how protozoan parasites regulate their lives. Trends Parasitol. *28*, 202–213.

De Gasparo, R., Halgas, O., Harangozo, D., Kaiser, M., Pai, E.F., Krauth-Siegel, R.L., and Diederich, F. (2019). Targeting a large active site: structure-based design of nanomolar inhibitors of *Trypanosoma brucei* trypanothione reductase. Chemistry *25*, 11416–11421.

Dejung, M., Subota, I., Bucerius, F., Dindar, G., Freiwald, A., Engstler, M., Boshart, M., Butter, F., and Janzen, C.J. (2016). Quantitative proteomics uncovers novel factors involved in developmental differentiation of *Trypanosoma brucei*. PLoS Pathog. *12*, e1005439.

Droll, D., Archer, S., Fenn, K., Delhi, P., Matthews, K., and Clayton, C. (2010). The trypanosome Pumilio-domain protein PUF7 associates with a nuclear cyclophilin and is involved in ribosomal RNA maturation. FEBS Lett. *584*, 1156–1162.

Ficarro, S.B., McCleland, M.L., Stukenberg, P.T., Burke, D.J., Ross, M.M., Shabanowitz, J., Hunt, D.F., and White, F.M. (2002). Phosphoproteome analysis by mass spectrometry and its application to *Saccharomyces cerevisiae*. Nat. Biotechnol. *20*, 301–305.

Field, M.C., Horn, D., Fairlamb, A.H., Ferguson, M.A., Gray, D.W., Read, K.D., De Rycker, M., Torrie, L.S., Wyatt, P.G., Wyllie, S., et al. (2017). Anti-trypanosomatid drug discovery: an ongoing challenge and a continuing need. Nat. Rev. Microbiol. *15*, 217–231.

Figueiredo, L.M., Cross, G.A., and Janzen, C.J. (2009). Epigenetic regulation in African trypanosomes: a new kid on the block. Nat. Rev. Microbiol. *7*, 504–513.

Haanstra, J.R., Gonzalez-Marcano, E.B., Gualdron-Lopez, M., and Michels, P.A. (2016). Biogenesis, maintenance and dynamics of glycosomes in trypanosomatid parasites. Biochim. Biophys. Acta *1863*, 1038–1048.

Jensen, R.E., Simpson, L., and Englund, P.T. (2008). What happens when *Trypanosoma brucei* leaves Africa. Trends Parasitol. *24*, 428–431.

Jones, N.G., Thomas, E.B., Brown, E., Dickens, N.J., Hammarton, T.C., and Mottram, J.C. (2014). Regulators of *Trypanosoma brucei* cell cycle progression and differentiation identified using a kinome-wide RNAi screen. PLoS Pathog. *10*, e1003886.

Kawahara, T., Siegel, T.N., Ingram, A.K., Alsford, S., Cross, G.A., and Horn, D. (2008). Two essential MYST-family proteins display distinct roles in histone H4K10 acetylation and telomeric silencing in trypanosomes. Mol. Microbiol. *69*, 1054–1068.

Kolev, N.G., Ramey-Butler, K., Cross, G.A., Ullu, E., and Tschudi, C. (2012). Developmental progression to infectivity in *Trypanosoma brucei* triggered by an RNA-binding protein. Science *338*, 1352–1353.

Kupferschmid, M., Aquino-Gil, M.O., Shams-Eldin, H., Schmidt, J., Yamakawa, N., Krzewinski, F., Schwarz, R.T., and Lefebvre, T. (2017). Identification of O-GlcNAcylated proteins in Plasmodium falciparum. Malar. J. *16*, 485.

Lai, D.H., Hashimi, H., Lun, Z.R., Ayala, F.J., and Lukes, J. (2008). Adaptations of *Trypanosoma brucei* to gradual loss of kinetoplast DNA: *Trypanosoma equiperdum* and *Trypanosoma evansi* are petite mutants of *T. brucei*. Proc. Natl. Acad. Sci. U.S.A. *105*, 1999–2004.

Langousis, G., and Hill, K.L. (2014). Motility and more: the flagellum of Trypanosoma brucei. Nat. Rev. Microbiol. *12*, 505–518.

Lueong, S., Merce, C., Fischer, B., Hoheisel, J.D., and Erben, E.D. (2016). Gene expression regulatory networks in Trypanosoma brucei: insights into the role of the mRNA-binding proteome. Mol. Microbiol. *100*, 457–471.

Manta, B., Comini, M., Medeiros, A., Hugo, M., Trujillo, M., and Radi, R. (2013). Trypanothione: a unique bis-glutathionyl derivative in trypanosomatids. Biochim. Biophys. Acta *1830*, 3199–3216.

Martinez-Calvillo, S., Romero-Meza, G., Vizuet-de-Rueda, J.C., Florencio-Martinez, L.E., Manning-Cela, R., and Nepomuceno-Mejia, T. (2018). Epigenetic regulation of transcription in trypanosomatid protozoa. Curr. Genomics *19*, 140–149.

Misra, K.K., Roy, S., and Choudhury, A. (2016). Biology of *Trypanosoma (Trypanozoon) evansi* in experimental heterologous mammalian hosts. J. Parasit. Dis. *40*, 1047–1061.

Mony, B.M., MacGregor, P., Ivens, A., Rojas, F., Cowton, A., Young, J., Horn, D., and Matthews, K. (2014). Genome-wide dissection of the quorum sensing signalling pathway in *Trypanosoma brucei*. Nature *505*, 681–685.

Moreno, S.A., and Nava, M. (2015). Trypanosoma evansi is alike to Trypanosoma brucei brucei in the subcellular localisation of glycolytic enzymes. Mem. Inst. Oswaldo. Cruz. *110*, 468–475.

Moretti, N.S., Cestari, I., Anupama, A., Stuart, K., and Schenkman, S. (2018). Comparative proteomic analysis of lysine acetylation in trypanosomes. J. Proteome Res. *17*, 374–385.

Mugnier, M.R., Cross, G.A., and Papavasiliou, F.N. (2015). The in vivo dynamics of antigenic variation in *Trypanosoma brucei*. Science *347*, 1470–1473.

Muller, L.S.M., Cosentino, R.O., Forstner, K.U., Guizetti, J., Wedel, C., Kaplan, N., Janzen, C.J., Arampatzi, P., Vogel, J., Steinbiss, S., et al. (2018). Genome organization and DNA accessibility control antigenic variation in trypanosomes. Nature *563*, 121–125.

Nett, I.R., Davidson, L., Lamont, D., and Ferguson, M.A. (2009a). Identification and specific localization of tyrosine-phosphorylated proteins in *Trypanosoma brucei*. Eukaryot. Cell *8*, 617–626.

Nett, I.R., Martin, D.M., Miranda-Saavedra, D., Lamont, D., Barber, J.D., Mehlert, A., and Ferguson, M.A. (2009b). The phosphoproteome of bloodstream form *Trypanosoma brucei*, causative agent of African sleeping sickness. Mol. Cell. Proteomics *8*, 1527–1538.

Picchi, G.F., Zulkievicz, V., Krieger, M.A., Zanchin, N.T., Goldenberg, S., and de Godoy, L.M. (2017). Post-translational modifications of *Trypanosoma cruzi* canonical and variant histones. J. Proteome Res. *16*, 1167–1179.

Ramos, T.C., Nunes, V.S., Nardelli, S.C., dos Santos Pascoalino, B., Moretti, N.S., Rocha, A.A., da Silva Augusto, L., and Schenkman, S. (2015). Expression of non-acetylatable lysines 10 and 14 of histone H4 impairs transcription and replication in Trypanosoma cruzi. Mol. Biochem. Parasitol. *204*, 1–10.

Rojas, F., Silvester, E., Young, J., Milne, R., Tettey, M., Houston, D.R., Walkinshaw, M.D., Perez-Pi, I., Auer, M., Denton, H., et al. (2019). Oligopeptide signaling through TbGPR89 drives trypanosome quorum sensing. Cell *176*, 306–317.e16.

Roy, N., Nageshan, R.K., Pallavi, R., Chakravarthy, H., Chandran, S., Kumar, R., Gupta, A.K., Singh, R.K., Yadav, S.C., and Tatu, U. (2010). Proteomics of *Trypanosoma evansi* infection in rodents. PLoS One *5*, e9796.

Sabari, B.R., Zhang, D., Allis, C.D., and Zhao, Y. (2017). Metabolic regulation of gene expression through histone acylations. Nat. Rev. Mol. Cell Biol. *18*, 90–101.

Siegel, T.N., Hekstra, D.R., Kemp, L.E., Figueiredo, L.M., Lowell, J.E., Fenyo, D., Wang, X., Dewell, S., and Cross, G.A. (2009). Four histone variants mark the boundaries of polycistronic transcription units in Trypanosoma brucei. Genes Dev. *23*, 1063–1076.

Siegel, T.N., Kawahara, T., Degrasse, J.A., Janzen, C.J., Horn, D., and Cross, G.A. (2008). Acetylation of histone H4K4 is cell cycle regulated and mediated by HAT3 in *Trypanosoma brucei*. Mol. Microbiol. *67*, 762–771.

Urbaniak, M.D., Martin, D.M., and Ferguson, M.A. (2013). Global quantitative SILAC phosphoproteomics reveals differential phosphorylation is widespread between the procyclic and bloodstream form lifecycle stages of *Trypanosoma brucei*. J. Proteome Res. *12*, 2233–2244.

Uzureau, P., Uzureau, S., Lecordier, L., Fontaine, F., Tebabi, P., Homble, F., Grelard, A., Zhendre, V., Nolan, D.P., Lins, L., et al. (2013). Mechanism of *Trypanosoma brucei gambiense* resistance to human serum. Nature *501*, 430–434.

Van Vinh Chau, N., Buu Chau, L., Desquesnes, M., Herder, S., Phu Huong Lan, N., Campbell, J.I., Van Cuong, N., Yimming, B., Chalermwong, P., Jittapalapong, S., et al. (2016). A clinical and epidemiological investigation of the first reported human infection with the zoonotic parasite *Trypanosoma evansi* in Southeast Asia. Clin. Infect. Dis. *62*, 1002–1008.

Vanhollebeke, B., Truc, P., Poelvoorde, P., Pays, A., Joshi, P.P., Katti, R., Jannin, J.G., and Pays, E. (2006). Human *Trypanosoma evansi* infection linked to a lack of apolipoprotein L-I. N. Engl. J. Med. *355*, 2752–2756.

Wang, W., Liu, F., Jiang, N., Lu, H., Yang, N., Feng, Y., Sang, X., Cao, Y., and Chen, Q. (2018). Plasmodium TatD-like DNase antibodies blocked parasite development in the mosquito gut. Front. Microbiol. *9*, 1023.

Wei, Y., Hu, H., Lun, Z.R., and Li, Z. (2014). Centrin3 in trypanosomes maintains the stability of a flagellar inner-arm dynein for cell motility. Nat. Commun. *5*, 4060.

Yang, Y., and Gibson, G.E. (2019). Succinylation links metabolism to protein functions. Neurochem. Res. *44*, 2346–2359.

Zhang, Y., Wang, X., Cui, D., and Zhu, J. (2016). Proteomic and *N*-glycoproteomic quantification reveal aberrant changes in the human saliva of oral ulcer patients. Proteomics *16*, 3173–3182.

Zheng, L., Jiang, N., Sang, X., Zhang, N., Zhang, K., Chen, H., Yang, N., Feng, Y., Chen, R., Suo, X., et al. (2019). In-depth analysis of the genome of Trypanosoma evansi, an etiologic agent of surra. Sci. China Life Sci. *62*, 406–419.

Zoltner, M., Leung, K.F., Alsford, S., Horn, D., and Field, M.C. (2015). Modulation of the surface proteome through multiple ubiquitylation pathways in African trypanosomes. PLoS Pathog. *11*, e1005291.

iScience, Volume *23*

Supplemental Information

Landscapes of Protein Posttranslational Modifications of African *Trypanosoma* Parasites

Naiwen Zhang, Ning Jiang, Kai Zhang, Lili Zheng, Di Zhang, Xiaoyu Sang, Ying Feng, Ran Chen, Na Yang, Xinyi Wang, Zhongyi Cheng, Xun Suo, Zhaorong Lun, and Qijun Chen

Supplemental Figures

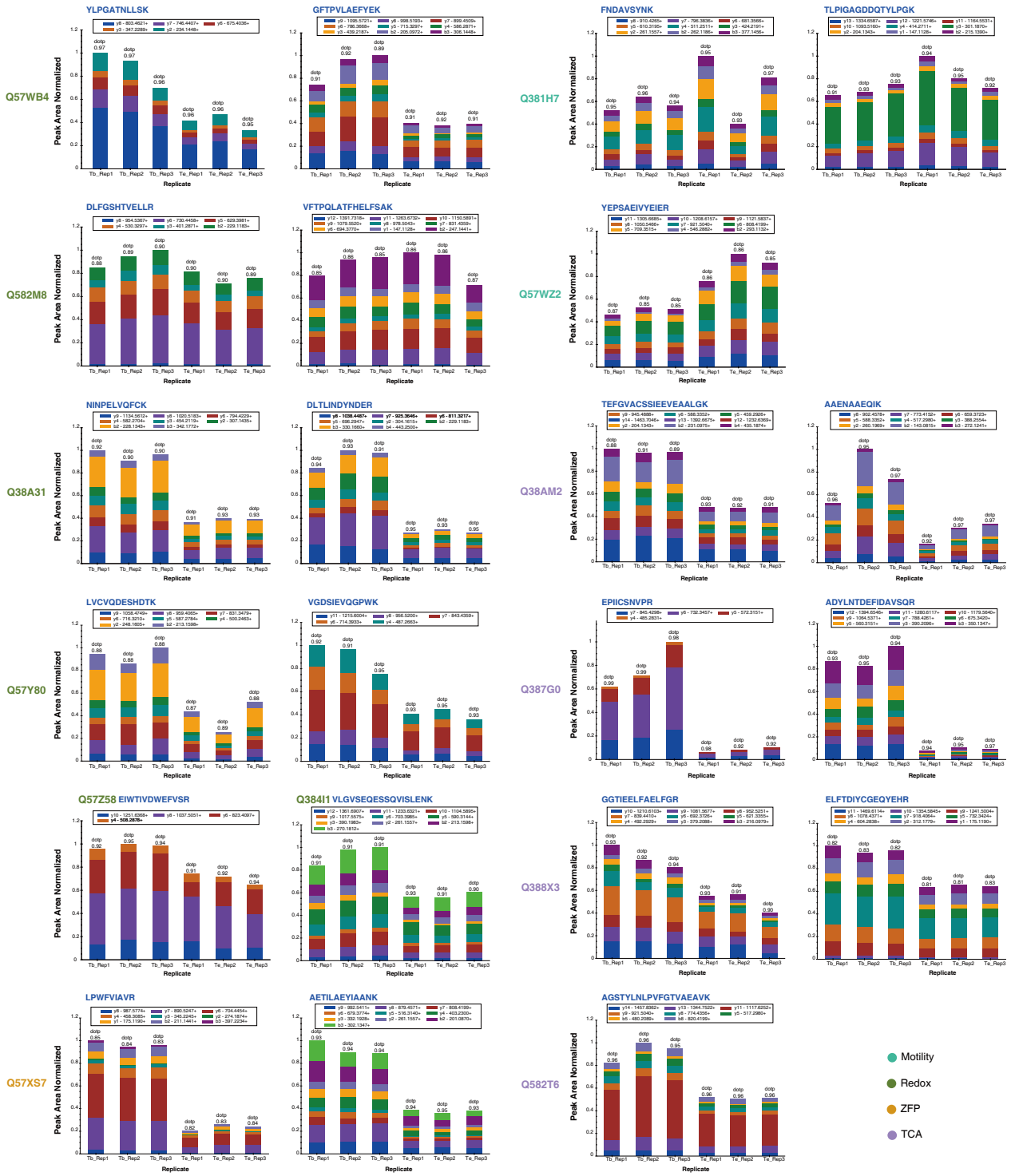

Figure S1. Target verification of proteomic data, related to Figure 1.

The peak area distribution of the fragment ion of the unique peptides of the selected target proteins. The peak area of the fragment ion was calculated by normalizing to the area of the internal standard for each sample.

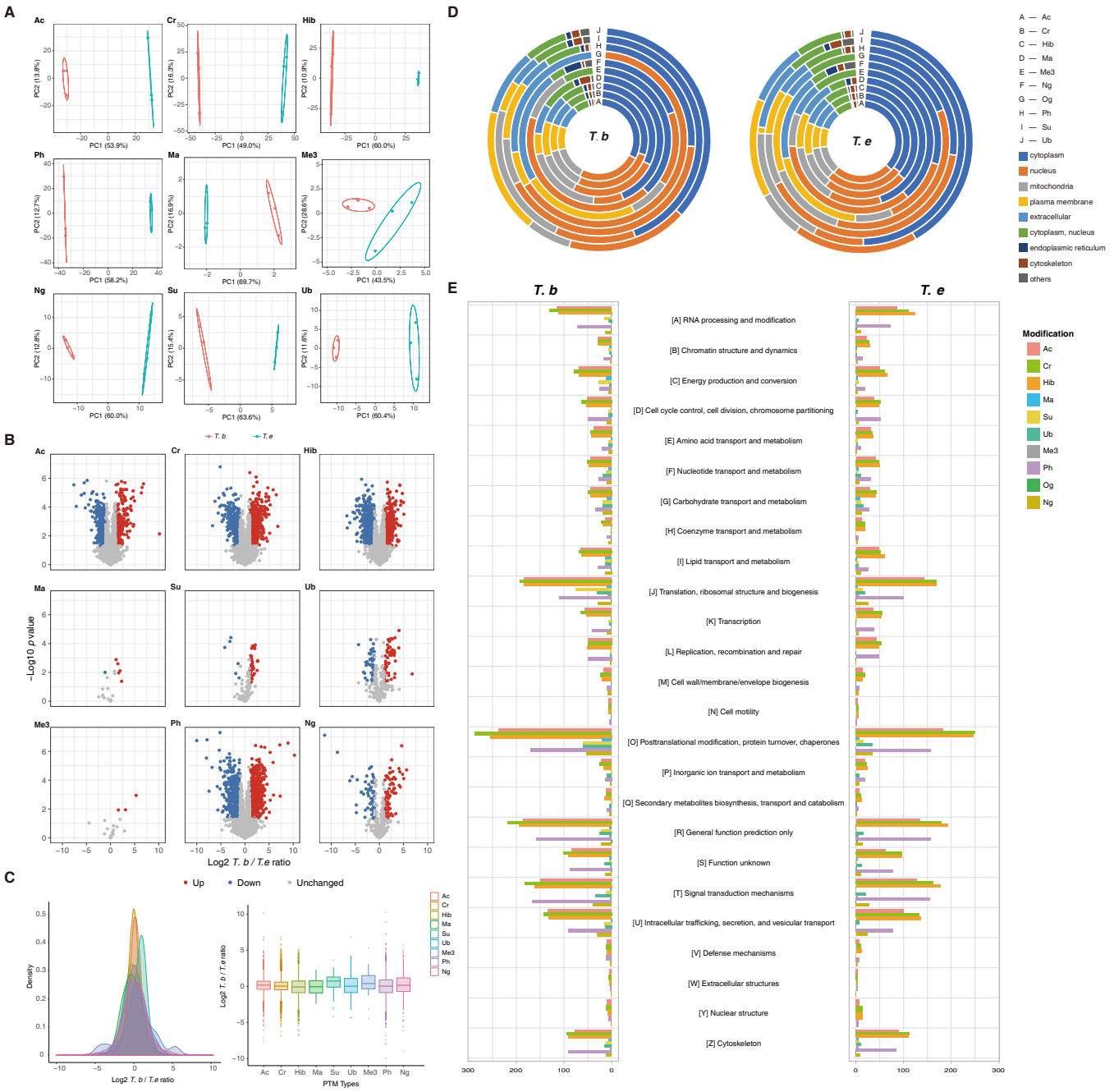

Figure S2. Qualitative analysis of differentially modified proteins in *T. brucei* and *T. evansi*, related to Figure 2.

(A) PCA of PTM-omes resulted in a clear separation of two groups which clustered tightly and represented the **3** eligible replicates of *T. brucei* and *T. evansi*.

(B) Volcano plot shows the distributions of quantified PTMs commonly identified in the two parasites. Highly modified proteins in *T. brucei* are shown in red, *T. evansi* in blue, and the unchanged proteins are shown in gray.

(C) Global distribution ratio for modified proteins in *T. brucei* and *T. evansi*.

(D) Subcellular structure prediction and classification statistics for proteins in different PTM-omes.

(E) Bar plots displaying KOG function distribution of the identified total proteins and modified proteins of *T. brucei* and *T. evansi*, respectively.

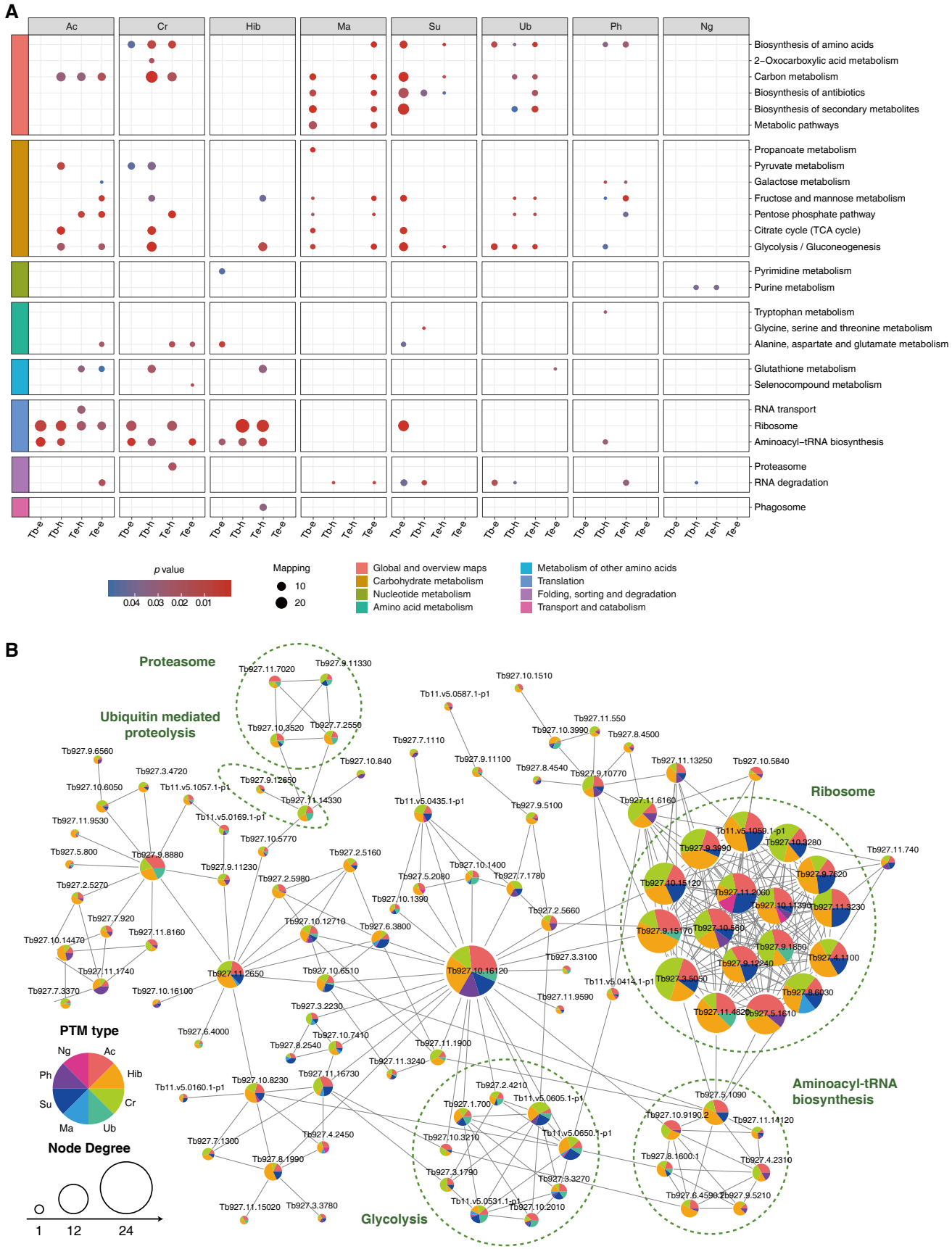

Figure S3. Quantitative analysis of differentially modified proteins in *T. brucei* and *T. evansi*, related to Figure 2.

(A) KEGG enrichment of proteins highlighting sets of pathways that are differentially modified in *T. brucei* and *T. evansi*. Heatmap colors represent log2 fold changes.

(B) Protein-protein interaction networks of differentially modified proteins; the interactive proteins are connected by lines, and the size of each protein node reflects the degree within the network. The colors of each node reflect which PTMs are differentially regulated.

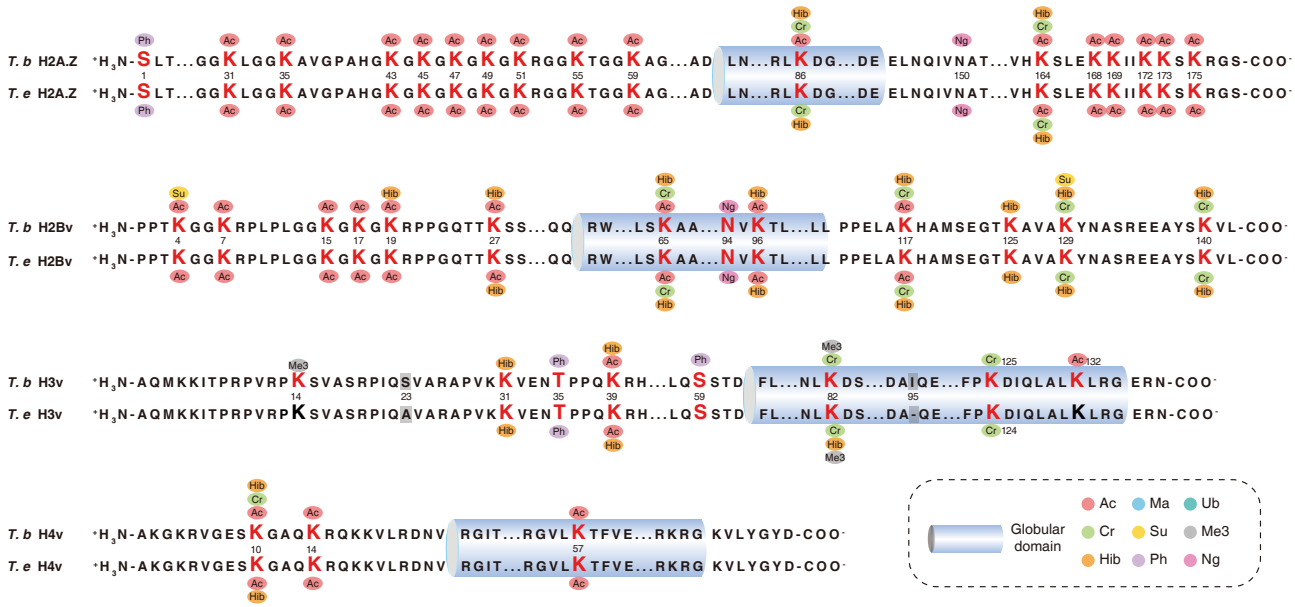

Figure S4. Variant histones are also heavily modified, related to Figure 3.

PTMs of variant histones for both *T. brucei* and *T. evansi*. Blue cylinders indicate the globular domains of histones. Sequences of mature histones are shown with the modified residues in bold (the numbers represent the amino acid position after removal of the initial methionine).

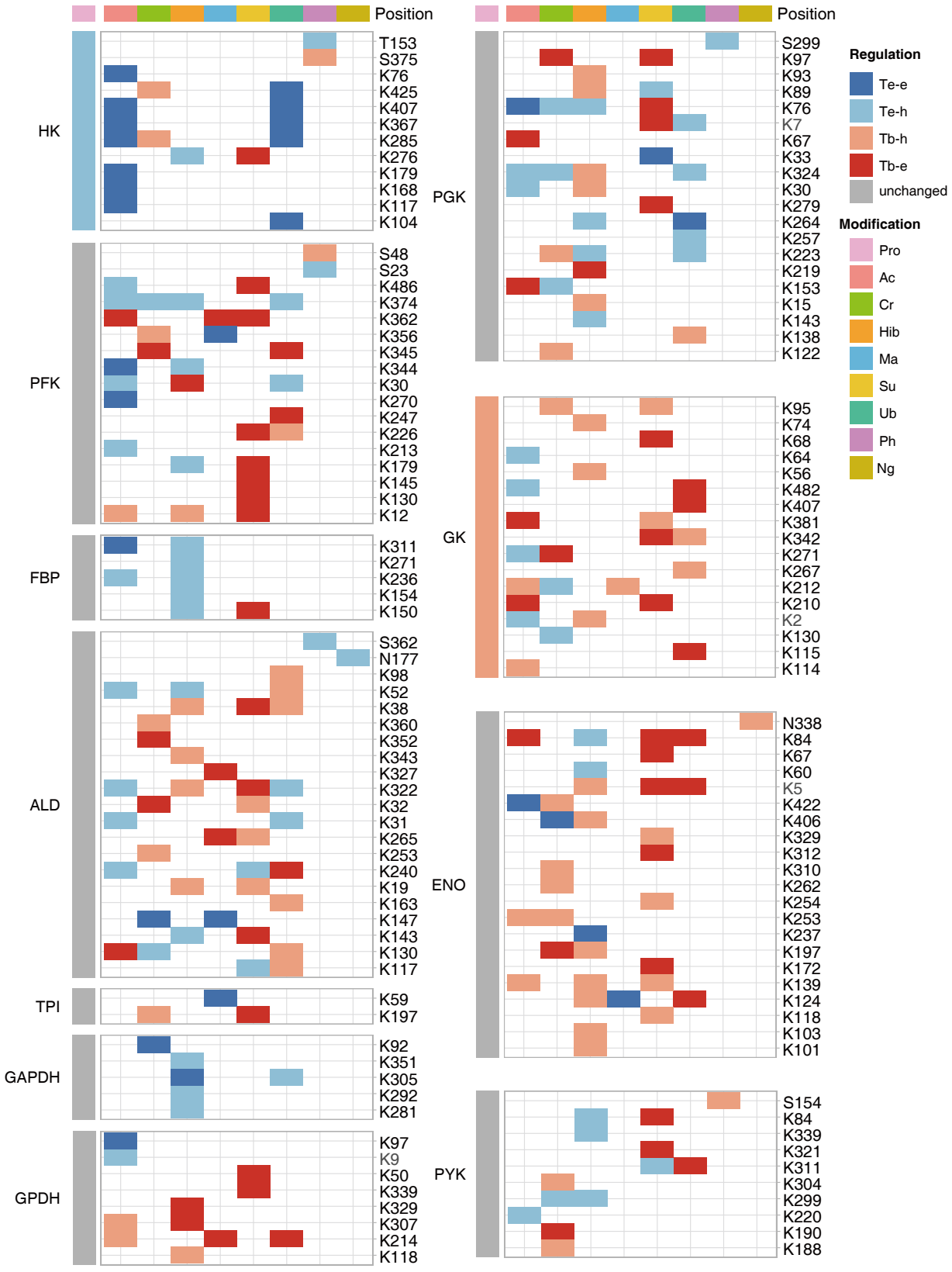

Figure S5. Glycolytic enzymes are differentially modified, related to Figure 7.

Heatmap displaying the variations of PTM types on all modified sites on the enzymes in the glycolysis pathway. The changed levels of kinases is indicated by the color of the vertical bar, and the levels of various modifications are indicated by the heat map. The modification types are color-coded.

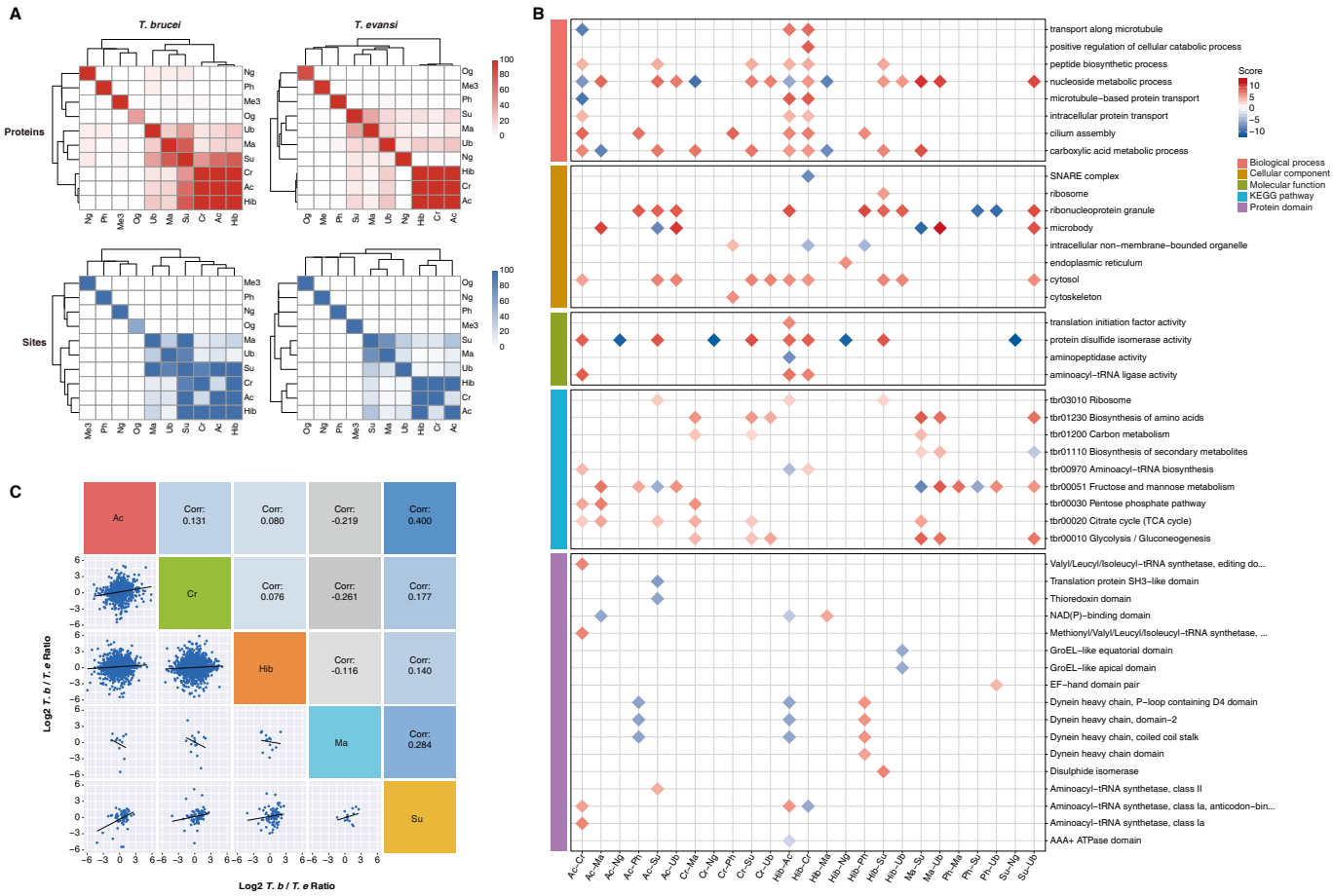

Figure S6. Crosstalk between different types of PTMs associated with critical biological processes, related to Figure 2.

(A) Heatmaps displaying the significance (-Log10 *p* value) of the overlaps of PTM datasets with one another.

(B) Crosstalk between the PTMs that occur on the proteins following enrichment of GO terms, KEGG pathways and domains. Heatmap displaying the normalized enrichment score; red indicates positive correlations and blue indicates negative correlations.

(C) The sites modified by different acylations were compared by 'one versus all' comparisons. Quantitative correlations between two modifications occurring at the same sites were evaluated using the Pearson correlation coefficient. The diagonal figures represent the relative quantitative abundance map of the modified sites. Scatter plots and Pearson correlations comparing individual replicate measurements are shown.

Transparent Methods

Ethics statement

Six- to eight-week-old pathogen-free female BALB/c mice were maintained in an enriched environment, and animal experiments were performed according to the institutional guidelines on animal welfare and ethical permissions. The study was approved by the Ethical Committee of Shenyang Agricultural University, China (Clearance number 2015-CAV-01).

Parasite cultivation and purification

T. brucei Lister 427 strain (Wirtz et al., 1999) and *T. evansi* YNB strain (Zheng et al., 2019) were maintained *in vivo* using BALB/c mice, and the trypanosomes were inoculated intraperitoneally into healthy mice for serial passage.

Trypanosomes were purified from the blood of infected mice over DEAE-cellulose (Sigma) when the parasitemia level reached 1×10^8 cells per ml (Lanham and Godfrey, 1970).

SDS-PAGE and Western blot analysis

The parasites were dissolved in SDS-PAGE loading buffer (250 mM Tris, 1.92 M glycine, and 1% SDS), electrophoresed on an SDS-PAGE gel and transferred to a 0.2-μm nitrocellulose membrane (Bio-Rad). After being blocked with Tris-buffered saline containing Tween 20 (TBST) and 5% skim milk (Sigma) for 1 h at 37°C, the membrane was incubated in TBST containing 5% skim milk and the anti-succinyllysine antibody (1:1,000 dilution; PTM BIO) for 12 h at 4°C. Next, the membrane was washed 5 times with TBST buffer and further incubated with horseradish peroxidase (HRP)-conjugated goat anti-mouse IgG (H+L) (1:10,000, Thermo Fisher Scientific). The membrane was incubated with the fluorogenic substrate (Millipore) for 5 minutes and the exposure time was adjusted according to the signal strength.

Immunofluorescence assay (IFA)

The smears of *T. brucei* and *T. evansi* were fixed with cold methanol in −80°C for 10 s and air dried. Next, the smears were washed three times using sterile phosphate-buffered saline (PBS) and blocked in 3% BSA for 1 h at 37°C, and the slides were incubated in PBS containing monoclonal pan anti-succinyllysine antibody (PTM BIO) for 12 h at 4°C. The smears were washed with PBS and further incubated with Alexa Fluor 488-conjugated goat anti-rabbit IgG (ThermoFisher Scientific) at 37°C for 1 h. The parasite nuclei were stained with DAPI (Invitrogen) for 5 min before image capturing with a fluorescence microscope (Leica).

Protein extraction

Parasites were incubated with a phenol extraction buffer (4-fold more buffer compared with parasite suspension) containing 10 mM dithiothreitol (Sigma), 1% protease inhibitors (Millipore), 1% phosphatase inhibitor (Millipore), 50 μM PR-619 (Selleck), 3 μM TSA (Selleck), 50 mM NAM (Sigma) and 2 mM EDTA; the mixture was ultrasonicated for 3 minutes, pause for 5 seconds per 3 seconds for 25% intensity. Next, an equal volume of Tris balance of phenol (Solarbio) was added and the mixture was centrifuged at 5,500 g for 10 min at 4°C. The supernatant was subsequently extracted and 5 times the volume of 0.1 M ammonium acetate/methanol was added for an overnight extraction; the precipitated protein was washed with methanol and acetone. Finally, 8 M urea was added to dissolve the pellet, and protein concentration was determined using the BCA kit (Beyotime).

Trypsin digestion

Dithiothreitol was added to the protein solution to a final concentration of 5 mM and reduced at 56°C for 30 min. Then, this mixture was alkylated with iodoacetamide (Sigma) to 11 mM for 15 min at room temperature in darkness. Finally, the urea concentration of the sample was diluted to less than 2 M by adding 100 mM NH_4HCO. Finally, trypsin (Promega) was added at a 1:50 trypsin-to-protein mass ratio for the first digestion

which was performed overnight at 37°C; a second 4 h-digestion was performed using a 1:100 trypsin-to-protein mass ratio.

HPLC Fractionation

The tryptic peptides (7.2 mg for phosphopeptides and 20 mg for others) were separated into fractions using high pH reverse-phase HPLC (Thermo Betasil C18 column, 5-μm particles, 10-mm i.d., 250-mm length). Briefly, peptides were first separated with a gradient of 8% to 32% acetonitrile (pH 9.0) over 60 min into 60 fractions. Then, the peptides were combined into 4 fractions and dried by vacuum centrifugation.

Affinity enrichment

For phosphorylation analysis, peptide mixtures were first incubated in an IMAC microsphere suspension with vibration in loading buffer; the loading buffer contained 50% acetonitrile (Fisher Chemical) and 6% trifluoroacetic acid (Sigma-Aldrich). The IMAC microspheres with enriched phosphopeptides were washed three times with a buffer solution containing 50% acetonitrile/6% trifluoroacetic acid and 30% acetonitrile/0.1% trifluoroacetic acid sequentially to remove nonspecifically adsorbed peptides. To isolate the enriched phosphopeptides from the IMAC microspheres, elution buffer containing 10% NH_4OH was added and the enriched phosphopeptides were eluted with vibration. The supernatant containing phosphopeptides was collected and lyophilized.

For *N*-glycosylation analysis, peptides were dissolved in the enrichment loading buffer (80% ACN/1% TFA) and the supernatant was subsequently pipetted into a hydrophilic HILIC microcolumn. After centrifugation at 4000 g for 15 min, the HILIC tip was washed three times with loading buffer. The glycopeptide was then eluted with 10% acetonitrile. Finally, the enriched glycopeptides were eluted with 80 μL of H_2O and lyophilized to dryness. For deglycosylation, 2 μL of PNGase F in 50 μL of 50 mM NH_4HCO_3 was added and the mixture was incubated at 37°C overnight (Zhang et al., 2016).

For analyses of acylation, ubiquitination, trimethylation, and *O*-GlcNAcylation, peptides were dissolved in IP buffer (100 mM NaCl, 1 mM EDTA, 50 mM Tris-HCl, 0.5% NP-40, pH 8.0) and the associated mixtures were incubated with pre-washed PTM-specific antibody conjugated beads (PTM BIO) at 4°C overnight with gentle shaking. Next, the beads were washed four times with IP buffer and twice with ddH_2O (Fisher Chemical). The bound peptides were eluted from the beads with 0.1% trifluoroacetic acid.

Finally, the eluted fractions were combined and vacuum-dried. For LC-MS/MS analysis, the resulting peptides were desalted with C18 ZipTips (Millipore).

LC-MS/MS Analysis

The tryptic peptides were dissolved in solvent A (0.1% formic acid) (Fluka), separated by an EASY-nLC 1,000 UPLC system and directly loaded onto a home-made reversed-phase analytical column (15-cm length, 75 μm i.d.). Solvent B was an aqueous solution containing 0.1% formic acid and 90% acetonitrile.

For proteome analysis, the gradient was comprised of an increase from 5% to 23% solvent B over 38 min, 23% to 35% for 14 min and climbing to 35% to 80% for 4 min, then holding at 80% for the last 4 min; a constant flow rate of 800 nL/min was used. For acylation, the gradient was comprised of an increase from 10% to 25% of solvent B over 38 min, 25% to 40% for 14 min and climbing to 40% to 80% for 4 min, then holding at 80% for the last 4 min, all at a constant flow rate of 700 nL/min. For detection of phosphorylation, the gradient was comprised of an increase from 3% to 25% solvent B over 62 min, 25% to 35% for 20 min and climbing to 35% to 85% for 4 min, then holding at 85% for the last 4 min, all at a constant flow rate of 700 nL/min. For ubiquitination, the gradient was comprised of an increase from 9% to 25% solvent B over 38 min, 25% to 40% for 14 min and climbing to 40% to 80% for 4 min and then holding at 80% for the last 4 min, all at a constant flow rate of 450 nL/min. For *N*- and *O*-glycosylation, the gradient was comprised of an increase from

8% to 23% solvent B over 38 min, 23% to 35% for 14 min and climbing to 35% to 80% for 4 min and then holding at 80% for the last 4 min, all at a constant flow rate of 450 nL/min.

The peptides were subjected to a nanospray ionization (NSI) source followed by tandem mass spectrometry (MS/MS) in Q Exactive™ Plus (Thermo) coupled online to the UPLC. The electrospray voltage that was applied was 2.0 kV. The m/z scan range was 350 to 1,800 for a full scan, and intact peptides were detected in the Orbitrap at a resolution of 70,000. Peptides were then selected for MS/MS using an NCE setting of 28 and the fragments were detected in the Orbitrap at a resolution of 17,500. A data-dependent procedure that alternated between one MS scan followed by 20 MS/MS scans with 15.0 s dynamic exclusion was employed. An automatic gain control (AGC) target of 5E4 was used. The signal threshold was set to 10000 ions/s, the maximum injection time was set to 100 ms, and the dynamic exclusion time of the tandem MS scan was set to 15 s to avoid duplicate scans of the parent ions.

Database searching

All MS/MS data were processed using the Maxquant search engine (v.1.5.2.8), and the spectra were searched against the UniProtKB database *Trypanosoma brucei brucei* (strain 927/4 GUTat10.1, 8,587 sequences, release time 2017.10) and NCBI database *Trypanosoma evansi* (strain YNB, 8,636 sequences, registration date 2019.1.23) (Zheng et al., 2019), and concatenated with a reverse decoy database. Trypsin/P was selected as a cleavage enzyme allowing up to two missing cleavages per phosphorylation and four missing cleavages for other reactions. The mass tolerance for precursor ions was set as 20 ppm in the First search and 5 ppm in the Main search, and the mass tolerance for fragment ions was set as 0.02 Da. Carbamidomethyl on Cys was specified as a fixed modification, and oxidation on Met and acetylation on protein N-terminus were specified as variable modifications. Additional variable modifications were specified for phospho-peptide analyses (phosphorylation of threonine, serine, and tyrosine residues), acetyl-peptide analyses (Kac), succinyl-peptide analyses (Ksu), malonyl-peptide analyses (Kma), ubiquit-peptide analyses (Kub), 2-hydroxyisobutyryl-peptide analyses (Khib), crotonyl-peptide analyses (Kcr), acetyl-peptide analyses (Kac), trimethyl-peptide analyses (trimethylation of lysine residues and trimethylation of arginine), and glycosyl-peptide analyses (*N*-glycosylation of asparagine residues and *O*-glycosylation of threonine, serine). FDR was adjusted to <1% and the minimum score for modified peptides were set >40. Minimum peptide length was set at 7. Label free quantification (LFQ) was selected for the quantification method. Specific mass of the modified peptides were matched to the corresponding proteomes to count the modification sites. All other parameters in MaxQuant were set to default values.

Parallel reaction monitoring (PRM)

The resultant MS data were processed using Skyline (v.3.6). Peptide settings: enzyme was set as Trypsin [KR/P], and Max missed cleavage was set as 0. The peptide length was set as 7-25, variable modification was set as Carbamidomethyl on Cys and oxidation on Met, and max variable modifications were set as 3. Transition settings: precursor charges were set as 2, 3, ion charges were set as 1, and ion types were set as b, y. The product ions were set as from ion 3 to the last ion, and the ion match tolerance was set as 0.02 Da.

Protein annotation and functional enrichment

GO annotation was derived from the UniProt-GOA database. For the proteins which were not annotated by the UniProt-GOA database, the InterProScan software was used to annotate each protein's GO function based on protein sequence alignment. Domain functional description was annotated by Interproscan, and the InterPro domain database was used. The KEGG online service tool KAAS was use to annotate the KEGG database description for proteins, and the annotation result was mapped on the KEGG pathway database using the KEGG service tool KEGG Mapper. Wolfpsort was used to predict subcellular localization. All functional enrichment was performed using a two-tailed Fisher's exact test. For further hierarchical clustering based on different protein

functional classification, all of the categories generated after enrichment along with their *P* values were collated; we subsequently filtered for those categories which were at least enriched in one of the clusters with a *P* value <0.05. This filtered *P* value matrix was transformed by the function x = −log10 (*P* value). Finally, these x values were z-transformed for each functional category. These z scores were then clustered by one-way hierarchical clustering (Euclidean distance, average linkage clustering) in Genesis. Cluster membership was visualized by a heat map using the "heatmap.2" function from the "gplots" R-package.

Identification of homologous proteins and PTM sites

The homologous proteins between *T. brucei* and *T. evansi* were determined using BLAST. All protein sequences from the two species were set as blast database files and query files. The blast output was defined as orthologous protein by filtration under the following conditions: E value < $1e^{-10}$, identity > 80, matched length coverage > 60% and mutual best hit between each other. MUSCLE (v. 3.8.31) was used to perform sequence alignment between homologous proteins. The simultaneous modified sites at the same position in homologous proteins were defined as the homologous PTM sites.

PTM site evolutionary conservation analysis

To estimate the degree of evolutionary conservation of PTM sites, a BLASTP analysis was used to compare the modified protein sequences identified in this study against protein sequences from 8 other species (*H. sapiens*, *S. cerevisiae*, *T. gondii*, *P. falciparum*, *L. major*, *T. gambiense*, *T. evansi* STIB805 and *T. cruzi*) using UniProtKB. MUSCLE (v3.8.31) was used to perform multiple sequence alignments. The conservation degree of modification sites for each species was calculated by counting the total number of conserved modified sites and the total number of conserved unmodified sites. An amino acid was considered to be conserved if it was identical in the aligned position of the query and the aligned species. The total number of the specific amino acid residues of proteins identified in this study was used as a control. *P* values were calculated using Fisher's exact test.

Phosphorylation motif analysis

Motif analysis was performed using motif-x (v1.2). Sequences were manually aligned and all proteins identified in our study were used as background. A width of 13 residues, a minimum number of 20 occurrences, and a significance of 0.00001 were specified before running motif-x.

Kinase-phosphosites regulated network

Identification of kinases was accomplished by alignment with Eukaryotic Kinase and Phosphatase Database (EKPD). The phosphosites phosphorylated by the relevant PK groups, families, or subfamilies were predicted by software GPS 2.0. We assumed that all the PKs in the same cluster would phosphorylate the sites. Thus, the protein-protein interaction (PPI) database was used as the major contextual factor to reduce false positive predictions.

Protein-protein interaction network

The differentially modified proteins, the previously predicted and annotated RNA-binding proteins (Lueong et al., 2016; Zheng et al., 2019), and kinases were searched against the STRING database (v11.0) to identify protein-protein interactions, respectively. Only interactions between the proteins belonging to the searched data set were selected, thereby excluding external candidates. STRING defines a metric called "confidence score" and this was used to define interaction confidence; all interactions that had a confidence score >0.7 (high confidence) were fetched. The interaction network from STRING was visualized in Cytoscape (v3.7.1).

Visual analysis of the three-dimensional structure of proteins

Information pertaining to the three-dimensional structure of proteins was searched against the PDB database by protein sequence, and the formatted three-dimensional structure file was visualized by UCSF ChimeraX.

Crosstalk analysis of different PTMs

The probability of different types of PTMs occurring on the same proteins were compared using Fisher's exact test *p* value, and the quantitative correlation between two types of PTM sites occurring on the same site were evaluated by the Pearson correlation coefficient.

Taking each two kinds of modification as a group, the terms with significant co-enrichment were selected, and the two enrichment results with specific modifications or high modifications in the same trypanosome were considered to have the same trend, namely positive regulation. By contrast, the others were considered to have the opposite trend, namely negative regulation. If the two modifications were positively regulated, Score was defined as the multiplied value of Fold enrichment. If negatively regulated, Score was defined as the negative of the value obtained by multiplying Fold enrichment.

Quantification and statistical analysis

Quantitative proteomic analysis was applied to *T. brucei* and *T. evansi* with three biological replicates performed for each, respectively. LFQ intensity and peptide intensity was used to calculate protein and modified quantitation, respectively. Quantitation ratios of homologous proteins and modified sites were generated from an average of three repeated intensities. The two-tailed *t*-test was applied to calculate the *p* value for significant differences. Proteins and modified sites with ratios of *T. brucei* / *T. evansi* > 2 and *p* values < 0.05 were regarded as being up-regulated, while proteins with ratios < −0.5 and *p* values < 0.05 were regarded as being down-regulated. Proteins and modified sites detected only in *T. brucei* and *T. evansi* with three replicates were regarded as *T. brucei*-specific and *T. evansi*-specific, respectively. Statistical significance of the survival rate was obtained with SPSS using the Log rank test.

Data and Software Availability

All data is available in the main text or the supplementary materials. The MS spectrometry measurement files have been deposited at the ProteomeXchange consortium (http://proteomecentral.proteomexchange.org) via PRIDE Archive (PXD016245).

Key resources table

REAGENT or RESOURCE	SOURCE	IDENTIFIER
Antibodies		
Anti-acetyllysine Antibody	PTM BIO	Cat# PTM-101
Anti-crotonyllysine Antibody	PTM BIO	Cat# PTM-502
Anti-2-hydroxybutyryllysine Antibody	PTM BIO	Cat# PTM-801
Anti-malonyllysine Antibody	PTM BIO	Cat# PTM-901
Anti-succinyllysine Antibody	PTM BIO	Cat# PTM-419
Anti-ubiquitin Antibody	PTM BIO	Cat# PTM-1106
Anti-trimethyllysine Antibody	PTM BIO	Cat# PTM-601
Anti-O-GlcNAc mouse mAb	PTM BIO	Cat# PTM-952
Goat anti-Rabbit IgG (H+L) Secondary Antibody, HRP	ThermoFisher Scientific	Cat# 31460
Goat anti-Mouse IgG (H+L) Secondary Antibody, HRP	ThermoFisher Scientific	Cat# 31430
Alexa Fluor™ 488 goat anti-mouse IgG (H+L)	ThermoFisher Scientific	Cat# A11029
Chemicals, Peptides, and Recombinant Proteins		
dithiothreitol	Sigma-Aldrich	Cat# 43815
PR-619	Selleck	Cat# S7130
NAM	Sigma-Aldrich	Cat# N5535
TSA	Selleck	Cat# S1045

Phenol	Solarbio	Cat# YZ-1524806
iodoacetamide	Sigma-Aldrich	Cat# I1149
trypsin	Promega	Cat# V5111
Water (HPLC)	Fisher Chemical	7732-18-5
acetonitrile	Fisher Chemical	75-05-8
trifluoroacetic acid	Sigma-Aldrich	Cat# 302031
formic acid	Fluka	Cat# 27001
salermide	Sigma-Aldrich	Cat# S8825
Critical Commercial Assays		
BCA kit	Beytime	Cat# P0012
DAPI	Invitrogen	Cat# D21490
Deposited Data		
Raw and analyzed data	This paper	PXD016245
Genome and RNA-binding proteins data of *Trypanosoma evansi*	Zheng et al., 2019	http://doi.org/10.1007/s11427-018-9473-8
The protein data of *Trypanosoma brucei*	UniProtKB	strain 927/4 GUTat10.1, release time 2017.10
RNA-binding proteins data of *Trypanosoma brucei*	Lueong et al., 2016	https://doi.org/10.1111/mmi.13328
Experimental Models: Organisms/Strains		
Trypanosoma brucei Lister 427 strain	Wirtz et al., 1999	N/A
Trypanosoma evansi YNB strain	Zheng et al., 2019	N/A
Pathogen-free female BALB/c Mouse	Liaoning Changsheng Biological Technology Company	N/A
Software and Algorithms		
MUSCLE (v. 3.8.31)	Edgar, 2004	http://www.drive5.com/muscle/
Skyline (v.3.6)	MacLean et al., 2010	https://skyline.ms
motif-x (v1.2)	Schwartz and Gygi, 2005	http://motif-x.med.harvard.edu
Maxquant search engine (v.1.5.2.8)	Cox and Mann, 2008	https://www.maxquant.org/
the UniProt-GOA database	The UniProt Consortium, 2017	http://www.ebi.ac.uk/GOA/
The STRING database (v11.0)	Szklarczyk et al., 2019	https://string-db.org/
Eukaryotic Kinase and Phosphatase Database (EKPD)	Wang et al., 2014	http://ekpd.biocuckoo.org/

Cytoscape (v3.7.1)	Shannon et al., 2003	https://cytoscape.org/
UCSF ChimeraX	Berman et al., 2019	http://www.rbvi.ucsf.edu/chimerax/
Other		
the three-dimensional structure of CRK3	PDB	PDB: 4GCJ
the three-dimensional structure of ALDO	PDB	PDB: 1F2J
the three-dimensional structure of ENO	PDB	PDB: 1OEP

Supplemental References

Berman, H.M., Adams, P.D., Bonvin, A.A., Burley, S.K., Carragher, B., Chiu, W., DiMaio, F., Ferrin, T.E., Gabanyi, M.J., Goddard, T.D., *et al*. (2019). Federating structural models and data: outcomes from a workshop on archiving integrative structures. Structure *27*, 1745-1759.

Cox, J., and Mann, M. (2008). MaxQuant enables high peptide identification rates, individualized p.p.b.-range mass accuracies and proteome-wide protein quantification. Nat. Biotechnol. *26*, 1367-1372.

Edgar, R.C. (2004). MUSCLE: multiple sequence alignment with high accuracy and high throughput. Nucleic Acids Res. *32*, 1792-1797.

Lanham, S.M., and Godfrey, D.G. (1970). Isolation of salivarian trypanosomes from man and other mammals using DEAE-cellulose. Exp. Parasitol. *28*, 521-534.

Lueong, S., Merce, C., Fischer, B., Hoheisel, J.D., and Erben, E.D. (2016). Gene expression regulatory networks in Trypanosoma brucei: insights into the role of the mRNA-binding proteome. Mol. Microbiol. *100*, 457-471.

MacLean, B., Tomazela, D.M., Shulman, N., Chambers, M., Finney, G.L., Frewen, B., Kern, R., Tabb, D.L., Liebler, D.C., and MacCoss, M.J. (2010). Skyline: an open source document editor for creating and analyzing targeted proteomics experiments. Bioinformatics *26*, 966-968.

Schwartz, D., and Gygi, S.P. (2005). An iterative statistical approach to the identification of protein phosphorylation motifs from large-scale data sets. Nat Biotechnol 23, 1391-1398.

Shannon, P., Markiel, A., Ozier, O., Baliga, N.S., Wang, J.T., Ramage, D., Amin, N., Schwikowski, B., and Ideker, T. (2003). Cytoscape: a software environment for integrated models of biomolecular interaction networks. Genome Res. *13*, 2498-2504.

Szklarczyk, D., Gable, A.L., Lyon, D., Junge, A., Wyder, S., Huerta-Cepas, J., Simonovic, M., Doncheva, N.T., Morris, J.H., Bork, P., *et al*. (2019). STRING v11: protein-protein association networks with increased coverage, supporting functional discovery in genome-wide experimental datasets. Nucleic Acids Res. *47*, D607-d613.

The UniProt Consortium. (2017). UniProt: the universal protein knowledgebase. Nucleic Acids Res. *45*, D158-D169.

Wang, Y., Liu, Z., Cheng, H., Gao, T., Pan, Z., Yang, Q., Guo, A., and Xue, Y. (2014). EKPD: a hierarchical database of eukaryotic protein kinases and protein phosphatases. Nucleic Acids Res. *42*, D496-502.

Wirtz, E., Leal, S., Ochatt, C., and Cross, G.A. (1999). A tightly regulated inducible expression system for conditional gene knock-outs and dominant-negative genetics in *Trypanosoma brucei*. Mol. Biochem. Parasitol. *99*, 89-101.

Zhang, Y., Wang, X., Cui, D., and Zhu, J. (2016). Proteomic and *N*-glycoproteomic quantification reveal aberrant changes in the human saliva of oral ulcer patients. Proteomics *16*, 3173-3182.

Zheng, L., Jiang, N., Sang, X., Zhang, N., Zhang, K., Chen, H., Yang, N., Feng, Y., Chen, R., Suo, X.*, et al.* (2019). In-depth analysis of the genome of *Trypanosoma evansi*, an etiologic agent of surra. Sci. China Life Sci. *62*, 406-419.